Modeling and simulation of the impacts of STATCOM control schemes on distance elements and control studies for a microgrid in a medium sized city in the Pacific Northwest

A Thesis

Presented in Partial Fulfillment of the Requirements for the

Degree of Master of Science

with a

Major in Electrical Engineering

in the

College of Graduate Studies

University of Idaho

by

Mohammed Fahad Allehyani

Major Professor: Brian K. Johnson, Ph.D.

Committee Members: Herbert Hess, Ph.D.; Ahmed Abdel-Rahim, Ph.D.

Department Administrator: Mohsen Guizani, Ph.D.

June 2016

Authorization to Submit Thesis

This thesis of Mohammed Allehyani, submitted for the degree of Master of Science with a major in Electrical Engineering and titled "Modeling and simulation of the impacts of STATCOM control schemes on distance elements and control studies for a microgrid in a medium sized city in the Pacific Northwest," has been reviewed in final form. Permission, as indicated by the signatures and dates given below, is now granted to submit final copies to the College of Graduate Studies for approval.

Major Professor: _____ Date: _____
Brian K. Johnson, Ph.D.

Committee Members: _____ Date: _____
Herbert Hess, Ph.D.

_____ Date: _____
Ahmed Abdel-Rahim, Ph.D.

Department Administrator: _____ Date: _____
Mohsen Guizani, Ph.D.

Abstract

This thesis encompasses two different subjects. The first is the performance of a distance protection scheme along with related supervisory elements are investigated when a shunt connected static synchronous compensator (STATCOM) is tapped to the midpoint of a transmission line. Different fault types are simulated while the STATCOM absorbs reactive power. The results show the distance relays tend to overreach when a STATCOM is injecting inductive current.

The second is part of an ongoing microgrid project that is held in a medium sized city in the Pacific Northwest. In this thesis, microgrid control studies are discussed for a medium sized city in the Pacific Northwest. General information about the microgrid concept and operation are provided. The study focuses on examining the microgrid behavior during varied system conditions. The results of the voltages and frequencies for both the grid and microgrid sides show the effect of the system conditions on the over/under voltage and frequency control schemes to detect conditions to prompt creation of islands. The performance of the generator control schemes and the benefits of load shedding are demonstrated.

Acknowledgements

First and foremost, praises and thanks to God, the Almighty, for providing me this opportunity and granting me the capability to proceed successfully.

I would also like to express my sincere gratitude to my major professor, Dr. Brian Johnson for being my mentor and guide all through my Master's program. Thank you for the patience, availability, enthusiasm, and advice you provided during my work. This helped me, to a great extent, in completing my thesis.

Also, I'm thankful to Dr. Herbert Hess and Dr. Ahmed Abdel-Rahim for their valuable time and insightful suggestions/questions, which motivated me to evaluate my work and thesis.

I would also like to thank the project sponsor for providing me this opportunity, and I extend my gratitude to the project teams for their cooperation.

I am also thankful to my fellow students, faculty, and staff of the ECE department who have been part of my Master's Degree completion.

Last but not the least, I would like to thank my family and friends, for their support and unwavering belief in me throughout my personal and academic life.

Dedication

"I dedicate this work to my parents, Fahad & Noor Allehyani, for all their love, prayers, caring, and sacrifices for educating and preparing me for my future, my dear wife, Rawan for her constant encouragement and support, and lastly my daughter, Shahad for the joy she makes in our lives."

Table of Contents

List of Figures

List of Tables

Acronyms

AC – Alternative Current

ATP – Alternative Transient Program

CERTS – The Consortium for Electric Reliability Technology Solutions

DC – Direct Current

DG – Distributed Generator Current

DLG – Double Line to Ground

DQ – Direct and Quadrature

DR – Distributed Resource

EMTP – Electromagnetic Transients Program

EPS – Electric Power System

FSC – Frequency Step Change

IEEE – The Institute of Electrical and Electronics Engineers

MVA – Megavolt Ampere

MVAR – Megavolt Ampere Reactive

MW – Megawatt

OUF – Over/Under Frequency

OUV – Over/Under Voltage

PCC – Point of Common Coupling

PLL – Phase Locked Loop

PU – Per Unit

PV – Photovoltaic

RLC – Resistor Inductor Capacitor

SCADA – Supervisory Control and Data Acquisition

SLG – Single Line to Ground

STATCOM – Static Synchronous Compensator

VSC – Voltage Source Converter

Chapter 1: Introduction

This chapter introduces the two topics of this thesis. The first topic is modeling and simulation of the impacts of STATCOM control schemes on distance elements, and the second topic is control studies for a microgrid in a medium sized city in the Pacific Northwest.

1.1. The Impacts of STATCOM Controls on Distance Protection Elements

The problem of uncertainty of operation for protection devices is a concern in the field of power systems. Distance protection schemes could experience uncertain operation with the presence of a STATCOM in the protected line. Therefore, the goal of this study is investigating the performance of a distance element when a STATCOM device is located in the middle of the line. This case is tested in the second chapter where an EMTP (Electromagnetic Transient Program)-type model is developed to simulate the power system and the impact of the control modes of the STATCOM. Also, a memory polarized distance relay, digital filter, supervisory element, and trip logic are modeled. Different simulation scenarios are tested and evaluated. The results show that distance relays tend to overreach when STATCOMs are injecting inductive current. After highlighting the problem and showing the results, Chapter 2 ends with a conclusion and suggested future work related to this study.

1.2. Microgrid Control Studies

The expansion of microgrid implementation and technology in real world power systems has increased recent years since 2003. Therefore, conducting well-planned studies and having insight and knowledge for the different contingencies in microgrid operation are

key factors in achieving successful microgrid operation that satisfies both the utilities and end users. Recently, research has been carried out in order to ensure optimal microgrid operation. Proper operation will lead to enhanced electric power sustainability and efficiency. The objectives of this thesis are investigating the grid connected and isolated operation of microgrid under varied system conditions, and developing a generator model with a detailed exciter and governor control circuits as well as modeling control schemes for monitoring the voltages and frequencies in the main grid and microgrid. The performance of these control schemes are tested and evaluated to ensure whether they were modeled and worked correctly or not. The arrangements of the microgrid topic in this thesis are as follows.

The concept of microgrids along with some leading projects and the different controls/operations of microgrid are described in Chapter 3 to give an overview about microgrid operation. The concept of synchronization and islanding detection schemes are highlighted in Chapter 4. Also, different synchronization and islanding detection methods are discussed. The test microgrid model along with the other control schemes are built in Chapter 5. A detailed model of the unit A machine in the microgrid is built along with over/under voltage frrequency tracking schemes and synchronization tracking control circuits are modeled in Chapter 5. The model is tested during three different cases: normal conditions, single line to ground (SLG) faults at different locations, and frequency swing conditions; the results are shown in Chapter 6. Finally, summary, conclusions, and future work are given in Chapter 7.

Chapter 2: The Impacts of STATCOM Controls on Distance Protection Elements

This chapter is based on a paper that was submitted to the 2016 North American Power Symposium, in Denver, Colorado. The paper's title is "Modeling and Simulation of the Impacts of STATCOM Control Schemes on Distance Elements". The paper is written by M. Allehyani, H. Samkari, and B.K. Johnson [1].

2.1. Introduction

Protecting transmission lines plays an important role in power systems. Distance protection schemes are widely used in transmission lines due to their effectiveness and capabilities [2]. Distance relays use both measured voltage and current to determine the approximate location of the fault, in tandem with high-speed protection zone reach and time-coordinated backup protection for adjacent lines [3]. In order to achieve a high level of sensitivity and reliability, distance relays are used along with supervisory overcurrent elements. However, there are many factors that could negatively impact distance protection. One is the presense of static synchronous compensators (STATCOMs) in transmission lines which may cause distance relays to maloperate.

A main objective of using STATCOMs in transmission applications is enhancing controllability and increasing the power transfer capability on transmission lines. STATCOMs can be controlled to absorb or supply reactive power independently, even during or after faults [4]. Distance relays may respond differently to faults as a result of the STATCOM's ability to provide instantaneous current compensation. Reference [5] states that distance relays will under-reach when STATCOMs are injecting capacitive current. On the other hand, distance

protection elements may overreach if STATCOMs are consuming reactive power. The distance relay would be most impacted when the STATCOM is located between the distance relay and the fault location [6], [7].

Reference [8] discusses the impacts of STATCOMs on the zone 1 reach of distance protection. The distance relay and the supervisory overcurrent element are examined when the STATCOM supplies reactive power. Different fault types are applied in different locations in order to test the system during fault conditions. The results show that the distance element under-reached for faults beyond the STATCOM. However, the relay was not affected when the faults occur between the STATCOM and the relay location. During the under-reaching case, the supervisory element measured reduced fault currents, which is the result of the STATCOM supplying capacitive current to the line. The study case consisted of a power system model with a STATCOM, STATCOM controls, and a relay model.

In this study, the impact of STATCOMs controlled to absorb reactive power on distance protection is discussed, and the role of the STATCOM controller in this interaction is explored. An AC voltage reference (V_{ref}) based controller attempts to maintain a set voltage at the PCC during fault events, whereas the reactive power reference (Q_{ref}) based controllers are set to maintain fixed reactive power [9]. The differences between these control modes impacts the relay response.

Distance relays are designed to act during faults in their proper zone. To improve security, distance relays are enhanced with a memory polarized quantity, which is essentially a buffer where the pre-fault voltage is saved in a memory filter to be used during fault events. This impact of the performance of two different STATCOM control schemes on memory polarized distance relay elements, and their supervisory elements will be characterized.

2.2. Study Case

This study focuses on the effect of a STATCOM on the zone 2 element of a distance relay while it absorbs reactive power. The study compares the relative impact between two common STATCOM control schemes since they tend to have different behaviors. Faults are applied beyond the reach setting of zone 2 (with faults located at 125% of line 1 impedance Figure 2.1).

Single line to ground (SLG), three phase, and double line to ground (DLG) faults are applied for each case. Phases B and C are chosen for DLG faults, and phase A to ground faults are chosen for SLG faults. For the three fault types, zero fault resistance (Rf = 0) is assumed.

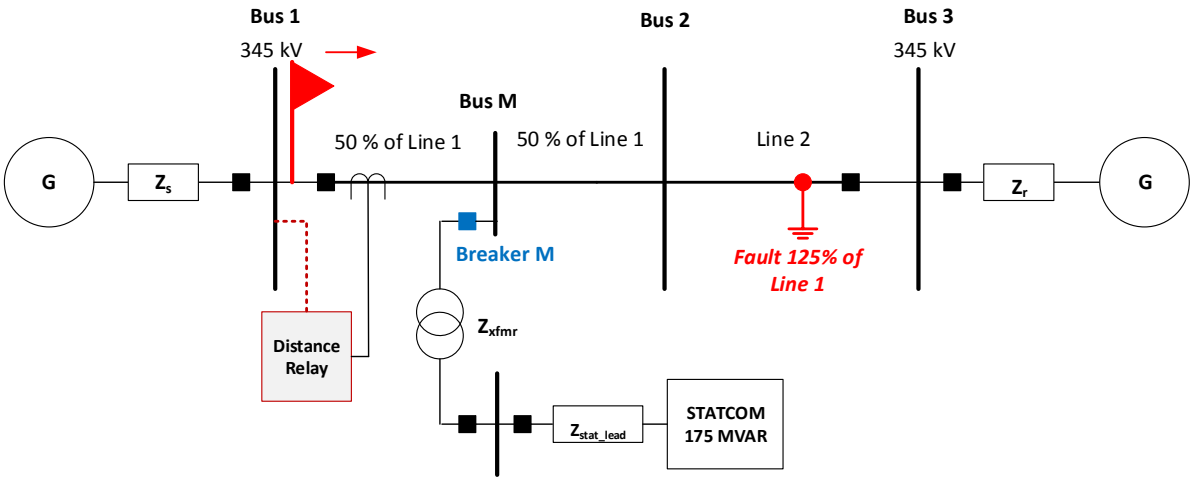

Figure 2.1. – Test Power System Diagram

The system is simulated in an Alternative Transient Program (ATP). After running the transient simulation, the data is exported to a Mathcad file. The data includes: three line currents, three line to ground voltages, and the neutral to ground current at the relay location

(BUS 1). A relay model is implemented in a Mathcad file that includes digital filters, distance relay elements, supervisory elements, and trip logic.

2.2.1. Model Description

A brief description of each model is discussed in this section. Three programs are used: ATP, Mathcad, and Powerworld. Figure 2.2 shows the process for each step of the simulations.

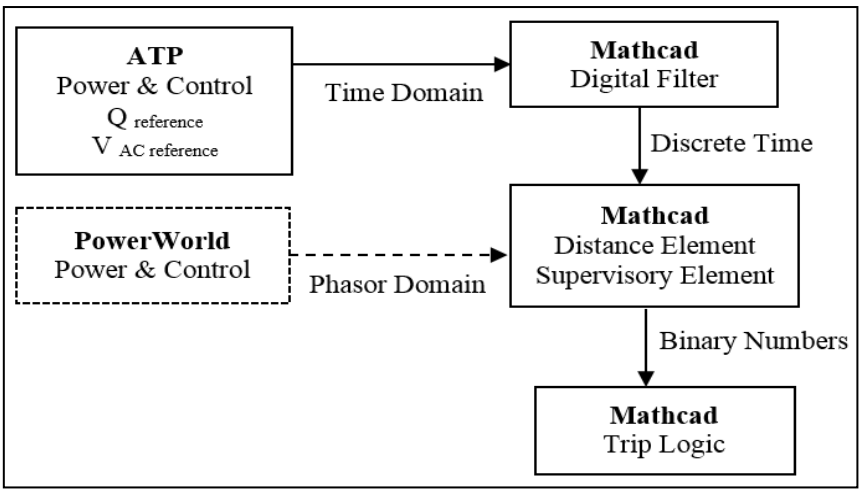

Figure 2.2. – Simulation Procedure Block Diagram

2.2.1.1. Power Model (ATP Model)

The system in Figure 2.1 is a 345 kV three phase system. The model consists of two equivalent source impedances, two fully transposed transmission lines, and a STATCOM connected to a tap at the midpoint of line 1. The transmission line models are based on a distributed parameters model assuming uniform transposition (appendix A provides more details) [6]. As shown in Figure 2.1, line 1 is between BUS 1 and BUS 2, and line 2 is between BUS 2 and BUS 3. The STATCOM is connected to the midpoint of line 1 through a 1:10

coupling transformer and an additional reactance. The STATCOM is absorbing 175 MVAR and 0 MW under light system loading condition. The three types of faults are applied at 125% of line 1 impedance. The relay is connected to BUS 1 looking to transmission lines (assuming ideal current and voltage transformers).

2.2.1.2. Relay Model (Mathcad Model)

The Mathcad file has digital filters, distance elements, supervisory elements, and trip logic functions. The digital filtering process takes the ATP data and resamples it at 16 samples per cycle. The next step is applying an averaging low pass filter with a cutoff frequency at 1/2 the sampling frequency, since the 60 Hz component is the desired component for the relay. The data is taken through a full cycle cosine filter. A sine filter is approximated by delaying the cosine filter output by a quarter cycle. The magnitudes and angles of the phase voltages, currents, and the zero sequence current at BUS 1 are obtained for each case.

The next step applies the measurements to a mho element implemented using a relay reach equation (here referred to as an m-equation, equation (2.1)). The distance element has two zones in its reach settings as shown in Figure 2.3, which shows a self-polarized mho circle for viewing simplicity. Zone 1 has been set to reach 85% of the total line 1 impedance, and zone 2 has been set to reach 120% of line 1. The distance relay element trip logic utilizes a positive sequence memory polarization quantity for the mho element. In addition, the M_{PhG} equation (2.1) has been calculated to find the distance to the fault location in per unit of the positive-sequence impedance, and comparing it to the reach setting [3]. The phase A to ground reach is calculated for SLG and three phase faults, and the phase C to ground loop is used for DLG faults since the fault resistance is assumed to be zero.

$$M_{PhG} = \frac{Re[V_{LG} * V_{LG\ mem\ pol}{}^{*}]}{Re[(e^{\Theta Zline}) * (I_{Ph} + (3 * I_0 * K_0)) * V_{LG\ mem\ pol}{}^{*}]} \quad (2.1)$$

Where,

M_{PhG}: the distance to the fault (phase to ground loop)

V_{LG}: line to ground voltage

$V_{LG\ mem\ pol}$*: pre-fault line to ground voltage (conjugate)

I_{Ph}: phase current

I_0: zero sequence current

K_0: zero sequence compensation factor

Θ_{Zline}: the angle of the line positive-sequence impedance

$$K_0 = \frac{Z_{line0} - Z_{line1}}{3\ Z_{line1}} \quad (2.2)$$

Where,

Z_{line0}: zero sequence line impedance

Z_{line1}: positive sequence line impedance

Equation (2.1) determines the effective impedance that is seen by the relay to the fault location based on the positive-sequence line 1 impedance. The zero sequence compensator factor for this system is K_0=0.597+j0.13 based on equation (2.2). The response of the effective impedance for a fault at 125% and the digital filter behaviour are shown in an impedance plane characteristic and compared to a mho circle. The effective impedance of a memory polarized element can be expressed by using equation (2.1) and represented in M plots versus

time. When the calculated effective impedance is less than the zone 2 setting, the trip logic will start a timer, and once that timer expires it will send a trip signal to BUS 1 circuit breaker to trip. On the other hand, the relay will not trip when the measured impedance is above the threshold or below zero.

The trip logic requires both the phase distance element and supervisory element to assert simultaneously. This is similar for ground distance element and ground distance supervisory elements.

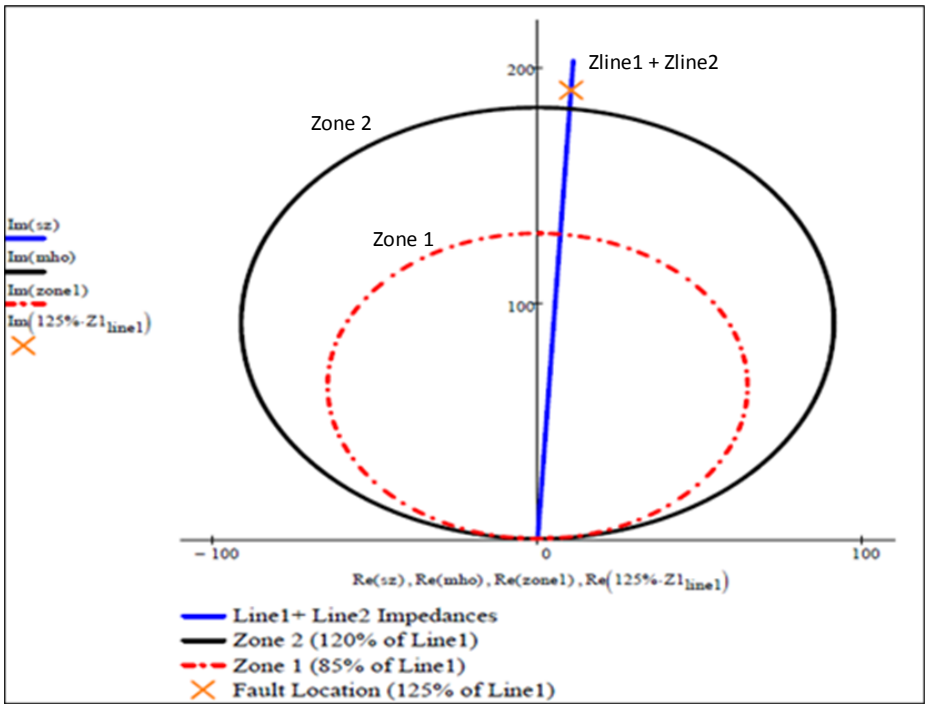

Figure 2.3. – Zone 1 and Zone 2 Mho characteristic

2.2.1.3. STATCOM Models (ATP Model)

The STATCOM models include two closed loop current regulated control schemes, one of which regulates the DC voltage, and the other is set to regulate either AC voltage

magnitude relative to reference voltage (V_{ref}) or reactive power relative to reference reactive power (Q_{ref}). The V_{ref} controller functions to maintain the voltage at the PCC at a set magnitude. However, in both schemes a fixed reactive power reference is used to obtain the q-axis current reference in the Q_{ref} controller (see Figure 2.4). In the case of Q control, a fall in the voltage at the PCC will change the current injection to maintain reactive power rather than regulate voltage.

Both control schemes use the measurements from the DC bus in order to regulate the DC bus voltage, and to find the direct current for the real power reference in the controller. This current should be zero if the losses are neglected, and this current loop regulates real power to supply converter losses when losses are modeled. The STATCOM converter is represented using a two-level, three phase DC/AC voltage source converter VSC implemented using an averaged model [9]. An averaged VSC model offers a good approximation in order to characterize the STATCOM performance under the circumstances studied [9].

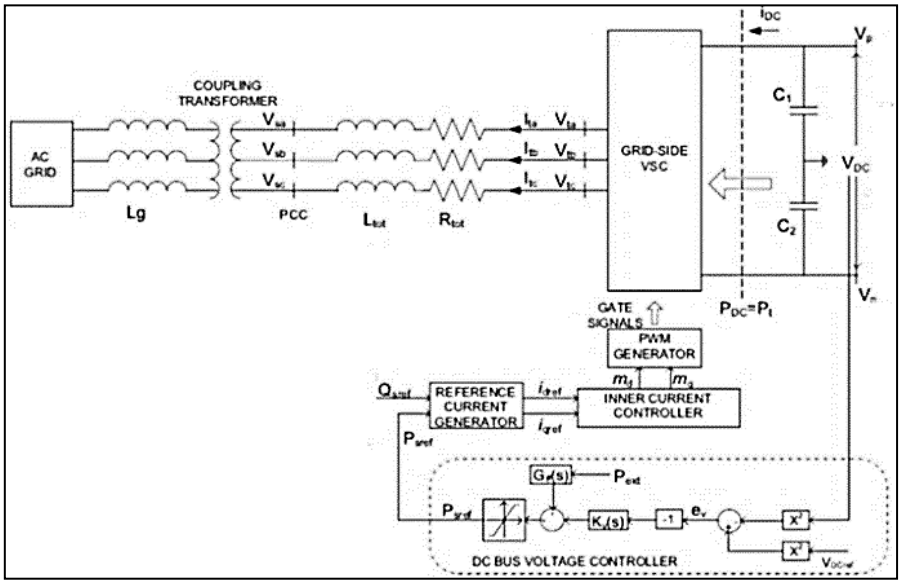

Figure 2.4. – Schematic Diagram of STATCOM and Controls [8]

2.2.2. Model Validation

First, a Powerworld model is utilized in order to validate the steady-state behavior of the ATP model and the Mathcad digital filter function. The Powerworld model provides magnitude and angle of the phase voltages, currents, and zero sequence current at the relay location (BUS 1) for each case. The STATCOM is represented as a synchronous condenser in Powerworld to assess the control system steady-state performance. The imported data is used to calculate the distance to the fault by using equation (2.1). The outcomes from the Powerworld model and the steady-state response ATP model show comparable results.

2.3. Simulation Results

The results of the fault types studied were fairly consistent, therefore only results for SLG faults at different locations have been chosen to show the behavior of the distance elements in Figures 2.5 and 2.6. The simulation results are summarized in Table 2.1, followed by a discussion of results.

As mentioned previously, the faults are applied in line 2 at 125% of line 1 impedance as seen from Bus 1, and the zone 2 distance relay is set at 120% of line 1 as seen from BUS 1. Figure 2.5 (a) shows the distance relay response for the fault without the STATCOM. Figure 2.5 (b) shows the impact of the STATCOM on the mho element while the STATCOM is controlled by Q_{ref} control scheme.

In Figure 2.6, the V_{ref} control scheme is used for the STATCOM. Since the load plays an important role in the relay decision in this control scheme, two load levels are applied. Figure 2.6 (a) shows the case when the load is normal (same load when the Q_{ref} control scheme is used). Figure 2.6 (b) shows the behavior of the relay when the transmission lines are heavily

loaded. During V_{ref} control scheme, the STATCOM is forced to maintain a voltage reference, this will lead the STATCOM to supply some reactive power as shown in Figure 2.8 (a).

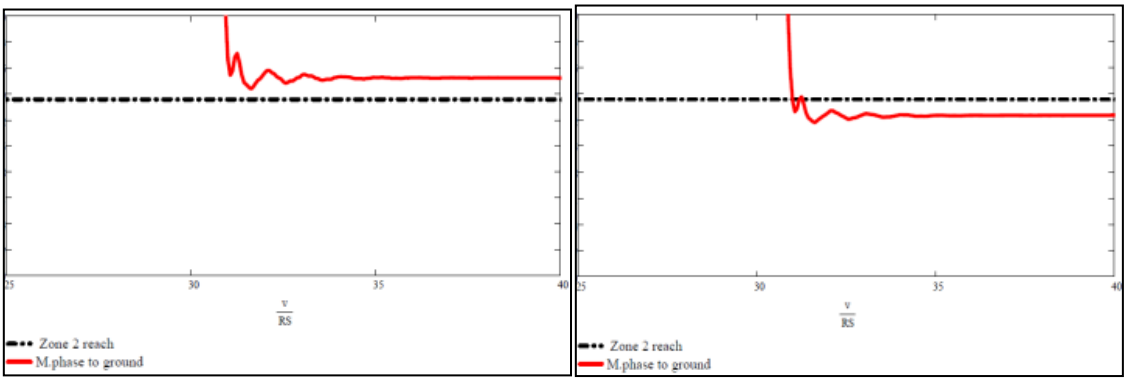

(a) Without STATCOM (b) With STATCOM

Figure 2.5. – The Distance to the SLG Fault Location Seen by the Relay (STATCOM Control Based on Q Reference)

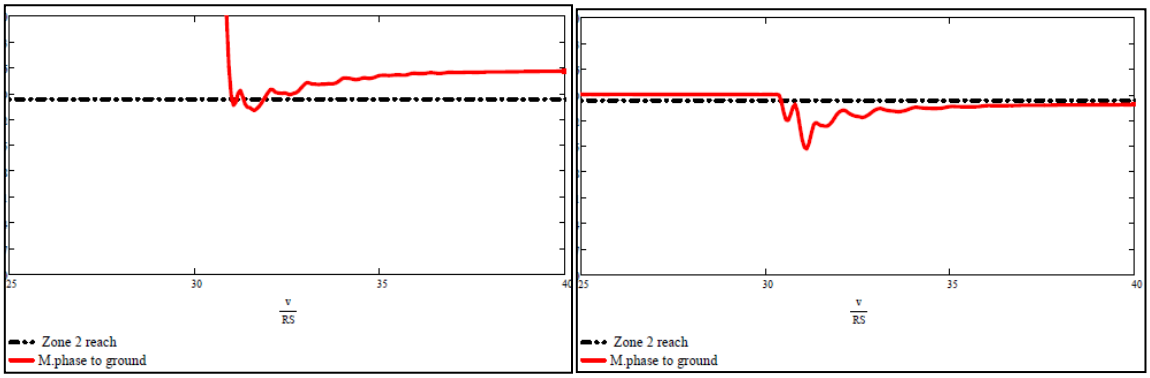

(a) Normally Loaded (b) Heavily Loaded

Figure 2.6. – The Distance to the SLG Fault Location Seen by the Relay (STATCOM Control Based on V Reference)

Table 2.1 – Summary of Results

Fault Type	**Control Scheme**		
	Q reference	***V reference***	***V reference Heavily Loaded***
SLG	Overreach	May overreach	More likely to overreach
DLG	Overreach	May overreach	More likely to overreach
Three Phase	Overreach	May overreach	More likely to overreach

2.3.1. Discussion of Results

The results are summarized as below:

- The Q_{ref} control scheme has the main impacts:
    - The distance relay overreaches when faults are applied at 125% of line 1 (STATCOM is connected and absorbs Q) see Figure 2.5 (b).
    - The STATCOM absorbs almost the same reactive power during normal and fault conditions as shown in Figure 2.7.
    - There are no significant differences in effect on the distance relay with different load and fault types.
- Main points for the V_{ref} control scheme:
    - The relay may or may not overreach when the transmission lines are lightly, or normally loaded Figure 2.6 (a).
    - The distance relay is more likely to overreach in the heavily loaded case Figure 2.6 (b).

- During fault events the STATCOM will absorb or supply reactive power as needed to regulate the voltage at the point of common coupling. The magnitude of the current injection has an impact on the relay response. For cases where the line is heavily loaded, the reactive current was larger and led to an overreach as shown in Figure 2.6 (b) and Figure 2.8 (b).
- In a normally loaded case, the voltage reference set point can be much higher than the voltage at the PCC during fault events. The controller will try to maintain the voltage at the PCC; as a result, the STATCOM will supply some reactive power and the distance relay may not overreach see Figure 2.6 (a) and Figure 2.8 (a).
- Fault types of SLG, DLG, and three phase have slight impact on the relay behavior.

- Trip logic commands are usually set to require two or three consecutive processing intervals below the threshold depending on the vendor, which might differentiate between the responses of the relays when V_{ref} control is used for fault regulation in the STATCOM since the threshold is not exceeded for long.

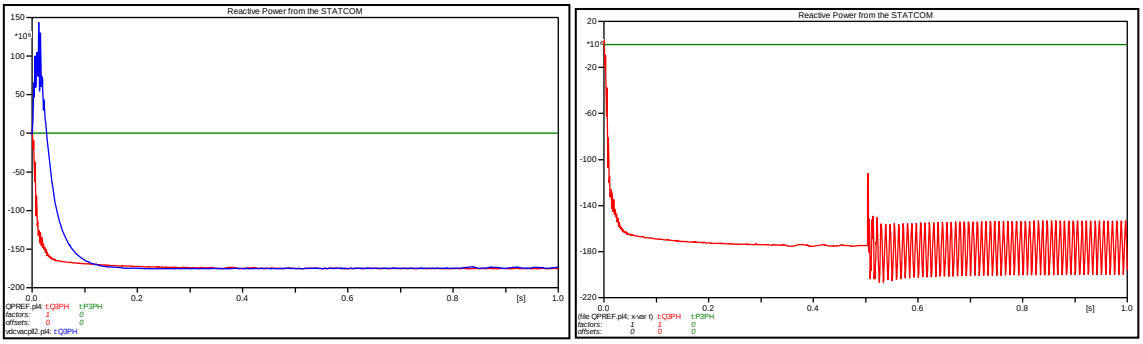

(a) No fault (b) With SLG fault at t=0.5s

Figure 2.7. – STATCOM Reactive Power Injection with Q_{ref} Control Scheme

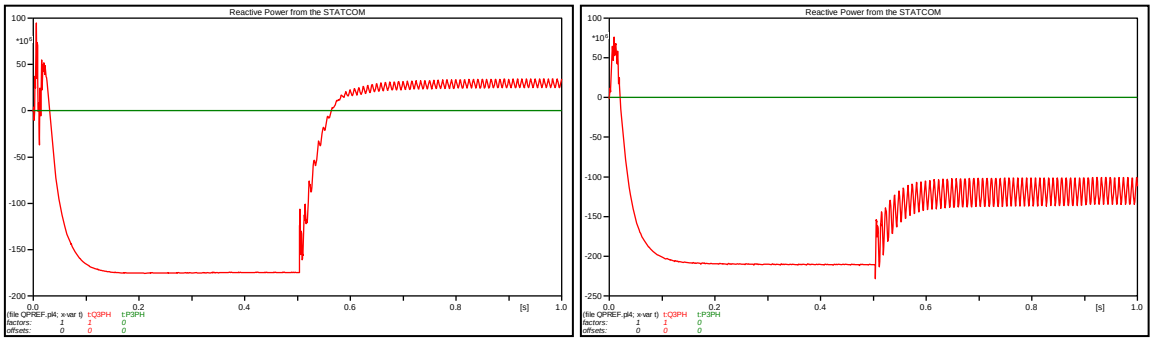

(a) Normally Loaded fault at t=0.5s (b) Heavily Loaded fault at t=0.5s

Figure 2.8. – STATCOM Reactive Power Injection with V_{ref} Control Scheme

- Figure 2.7 (a) shows two colors. The red color represents the STATCOM reactive power injection during Q_{ref} shceme, and the blue color represents the reactive power injection during V_{ref} control scheme.
- It was also observed that the supervisory element is affected because the STATCOM increases the fault current seen by the relay.

- Zone 1 of line 1 is also affected when the STATCOM is present in the fault loop. However, STATCOMs usually have a self-protection mode for close in faults and will trip off line.
- Figure 2.7 and 2.8 show a start-up behaviour for the time between (0 – 0.02 sec), so the only the period after 0.02 seconds matters.
- The ripples in Figure 2.5 and Figure 2.6 show the digital filter transient behavior.
- Comparable steady state results from ATP simulation and Powerworld validate the model.

2.4. Conclusion Related to the First Topic

This study has examined and discussed the performance of a distance protection scheme with supervisory elements while a STATCOM absorbs reactive power. The simulation results from the developed models show a relay overreaching problem when the STATCOM uses a Q_{ref} controller. On the other hand, when the STATCOM adopts V_{ref} controller, the overreach depends on the voltage at the PCC, and the prefault load current. While the STATCOM supplies reactive power, underreach is instead a problem [8]. The simulation results show that distance relays are mostly impacted when STATCOMs are inside the fault loop.

In order to mitigate the maloperation due to the underreach and overreach issues, establishing a communication channel between the relay and STATCOM location would be one of the solutions [10]. Since the STATCOM response only impacts the zone 2 element of the protection scheme in this study, there is potentially sufficient time for communication. If synchrophasor data is exchanged, the latency issues need to be considered [11]. STATCOMs

have different control schemes, and can alternate between two modes, so other control schemes should be investigated for future studies. Building upon the case study in this paper, the effects of fault resistance and the effects of weak sources should be considered. Also, applying load encroachment and communication aided distance elements are further enhancements.

Chapter 3: Overview of Microgrids

The 2003 blackout in the Northeast of America is considered a disaster in the U.S. More than 531 generators and 400 transmission lines were interrupted, causing more than 50 million people to be without electricity [15]. Such an event was investigated by the US government in order to avoid similar power outages in the future. The results of this investigation have shown that, "it is much easier and faster to develop distributed power than to reform the power grid to enhance security" [16]. Since then, the topic of microgrids has become a trend in literature. The basic concept of a microgrid involves small distributed generators (DGs) and a group of interconnected loads with or without energy storage that work in a decentralized control fashion. This group of loads with DGs works as a single controllable system with respect to the grid. (Figure 3.1).

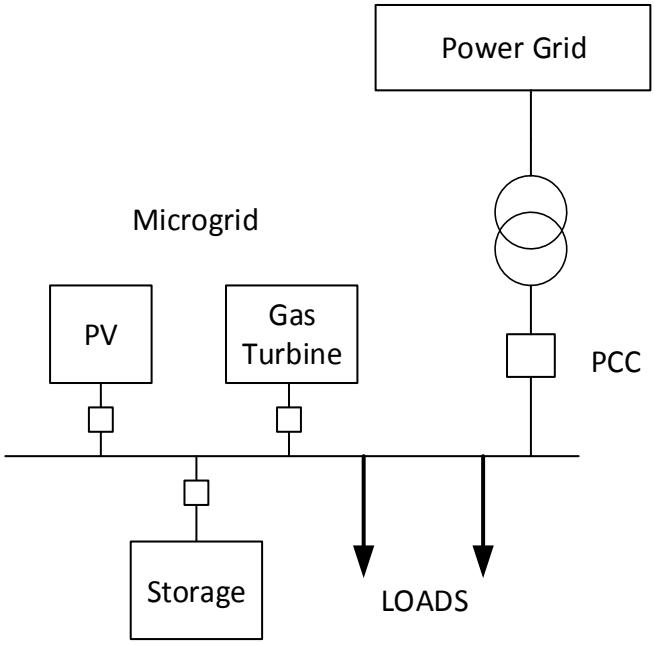

Figure 3.1 Example of Microgrid Structure

DGs are by definition connected to the distribution system and are often located close to the loads to increase the system's reliability, efficiency, and to minimize the loss of load. Also, carbon dioxide CO_2 emissions can be reduced through the use of DGs based on renewable energy sources (RES) such as solar-PV systems, wind turbines, and small hydro generators. Therefore, a more sustainable and resilient power system can be achieved by employing the idea of microgrids [17].

Microgrids can operate in two different modes with respect to the main power system: grid connected or islanded mode. In grid connected, parallel operation, power can be exchanged between the main grid and the microgrid. This offers an advantage as the microgrid contributes to cover part of the total demand and therefore reduce the peak point. In an isolated microgrid, the PCC circuit breaker to the main grid will be open to create a planned or unplanned island. The planned microgrid is a result of a scheduled microgrid where the time and duration of this event is arranged. The unplanned microgrid occurs when the electric power system (EPS) experiences an abnormal condition, and the islanding detection schemes (explained in Chapter 5) detect the loss of the grid to form an islanding microgrid. During autonomous microgrid operation, the DGs act as voltage controlled sources and regulate their terminal voltage. The DGs within the island should support the critical loads and maintain the electric power continuity [18]. The transition between a grid connected and an isolated microgrid should be as fast as possible to achieve a seamless transition. It requires this speed of action to maintain the system's stability and supply a high degree of power quality.

3.1. Example Microgrid Installations

For past ten years, industries, governments, researchers, and others have been conducting research and studies to apply the concepts of microgrid in the real world. Two examples are described below. The Consortium for Electric Reliability Technology Solutions (CERTS) is a leading organization in this field.

The main objective of the CERTS project is to apply the concept of a microgrid as shown in Figure 3.2 to have a reliable power supply for end users. The dynamic response of the microgrid was tested while having multiple inverter based DGs that combine heat and power sources. The project tested different scenarios that may occur in a microgrid during parallel or islanded modes. The static switch was examined to ensure a smooth transition between a stand-alone and grid connected modes. Also, system protection performance and the DGs response during various load conditions were recorded [19].

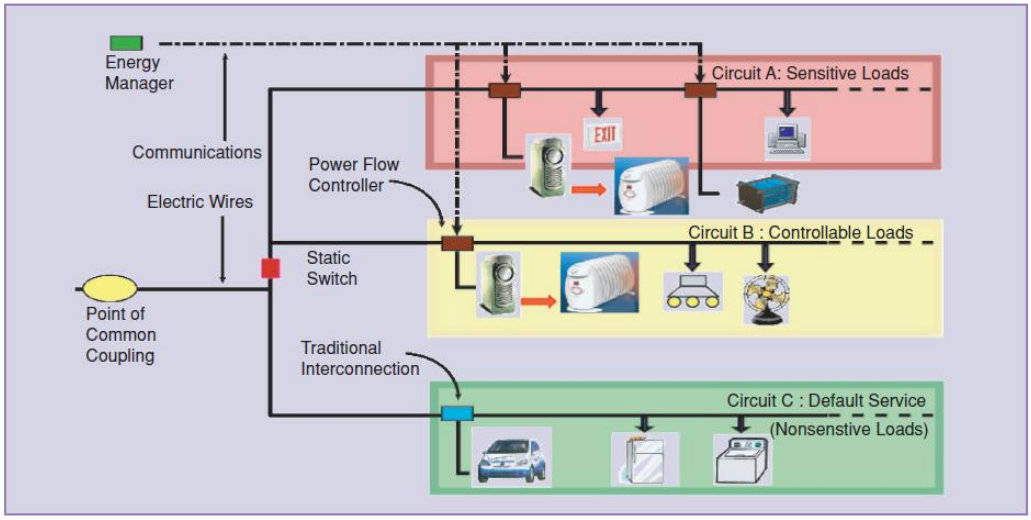

Figure 3.2 CERTS Microgrid Architecture [19]

BC Hydro's Boston Bar project in Canada is another project that applies the islanded microgrid concept as shown in Figure 3.3. The project aims to enhance the system reliability in the town of Boston Bar. The customers in town experienced frequent power outages each year, and travel to the city is fraught with risks due to weather conditions and nature of the area. Therefore, two hydro DGs were installed to cover the community's needs. The project studies the islanded system, resynchronization, and black start conditions [19].

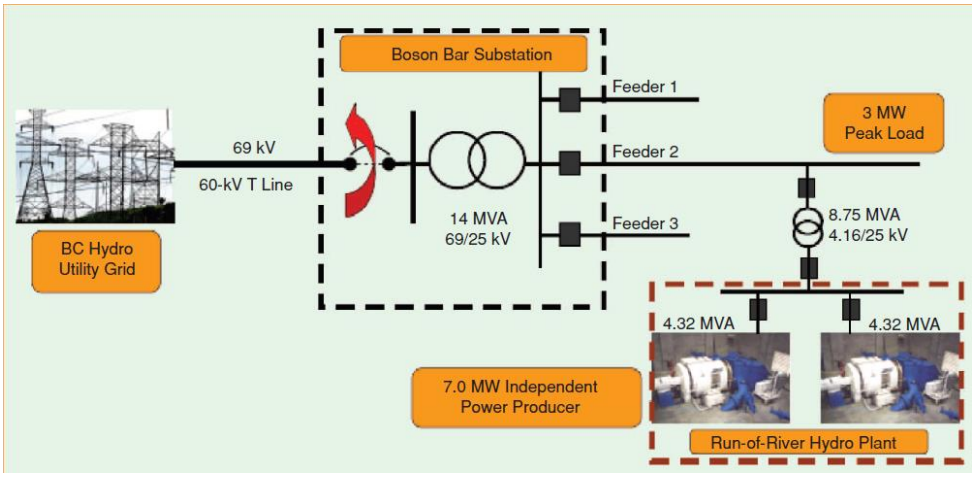

Figure 3.3 BC Hydro's Boston Bar islanding Microgrid [19]

3.2. Microgrid Control Strategies

Microgrid control operation depends on the microgrid connection. The DGs within the microgrid act according to the microgrid operation whether it is in grid connected or stand-alone mode. The different control strategies are described below.

3.2.1. Master/Slave Technique

The concept of the master/slave technique operates based on having a master microgrid controller at a master DG with all other sources acting according to commands from

the master unit. Which means that the other units are connected to the master unit via communication channels [20]. During parallel operation of the microgrid, there is no need for frequency regulation, however, in islanded operation, the master DG should regulate its output power as well as the other units' output power to control the variation of the load demand. Also, the master unit is responsible for maintaining the microgrid system frequency and voltage. The master DG then acts as voltage controlled source [20], [21]. One of the challenges of this method is that a failure on the master unit could impact the whole system [19].

3.2.2. Peer to Peer Technique

In the peer to peer control strategy, all of the DGs retain the same function, whether they are grid connected or in an islanded microgrid. Peer to peer means that DGs can be installed/operated with no changes in the grid control systems ("plug and play"). Unlike the master – slave technique, peer to peer requires no communications between the sources. Nevertheless, each unit independently responds to a system change which makes this control scheme cost effective. Peer to peer microgrids regulate voltage and frequency using droop control methods such as P/F droop scheme where the units try to maintain a set power as the frequency varies [22].

3.3. Microgrid Challenges

A number of challenges for microgrid operation have been raised and must be considered to accomplish a well-established microgrid. One of these considerations is the protection coordination between the relays within the microgrid. There needs to be differentiation between grid connected and islanded mode. The protection devices should account for the two-operating conditions. Many newer DGs are inverter based DGs with a

power electronic interface. This affects the system stability due to the lack of rotating masses and therefore less inertia support. And also complicated protection due to fault current limiting in the inverter.

The more DGs the more complexity is added to the system. Thus, a control scheme is needed to smoothly deal with multiple DGs. Maintaining the system frequency is a challenge that would affect the overall system, therefore regulating the grid voltage and frequency (as well as that of the microgrid) is a significant objective for the system stability. Also, proper detection for an islanding condition is important for the system security and safety. Both topics will be explained in the next chapter.

Chapter 4: Islanding Detection in a Microgrid and Synchronization

Connecting a microgrid to an existing grid requires a reliable synchronization technique. Also, during abnormal conditions while the microgrid is in grid-connected mode, the microgrid should detect and react to abnormal conditions to form an islanded microgrid. Those two topics will be discussed in this chapter.

4.1. Synchronization of a Microgrid to the Main Grid

The process of synchronizing two power systems is the process of matching voltage and frequency for the two systems, allowing them to work in parallel fashion. In this thesis, the scope is focused on the synchronization between the main grid and the microgrid. The parallelization condition between the synchronized systems achieves power sharing benefits while exchanging load flow [23]. To better understand synchronization, Figure 4.1 shows the phase sequence, voltage amplitude, frequency, and phase angle of the two systems. These values should be equal, with an acceptable tolerance, across the point where the two systems would be connected prior to closing the breaker.

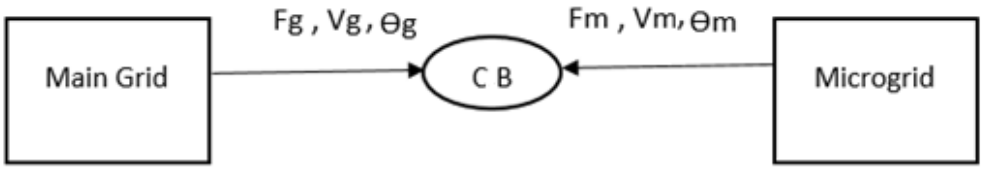

Figure 4.1: The Basic Concept of Microgrid Synchronization

Where,

F_g, F_m: main grid and microgrid frequencies (Hz)

V_g, V_m: main grid and microgrid voltage amplitudes (kV)

Θ_g, Θ_m: main grid and microgrid phase angles (degree)

C B: intertie circuit breaker

Successful synchronization is a crucial factor in power systems. Avoiding the detrimental consequences of a failed synchronization will prevent equipment damage, loss of power, and safety risks. The synchronization method should be chosen depending on the rating of the machines available and the system control behavior.

4.1.1 Synchronization Methods

According to IEEE1547 [18], there are two classes of recommended techniques that could be used for synchronizing a distributed resource DR with the EPS: manual and automatic. Both methods achieve the same goal of closing the intertie circuit breaker to have the two system working in synchronism.

4.1.1.1 Manual Synchronization

This method is not common and is only used with low rating DR [18]. Corresponding to its “manual” name, the job relies on an operator who is responsible for achieving the operation. In addition to the human factor in this method, a synchronism check relay is used to back up the operator’s closing decision. The basic operation concept of the manual synchronization method is illustrated in Figure 4.2. The voltage, frequency, and phase angle

are monitored by a voltmeter, a frequency meter and a synchroscope. When the voltage and frequency within the acceptable range, and the synchroscope is on the 12 O'clock position, the operator initiates a close command. The synch check relay element, device 25 is used to prevent closing the circuit breaker outside the acceptable range. Reference [18] provides more details on the regulations of using manual synchronization in a microgrid.

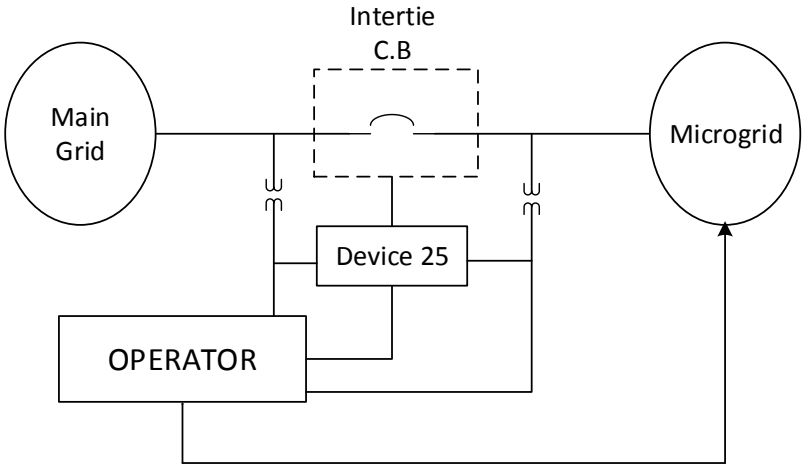

Figure 4.2 – Manual Synchronization Diagram

4.1.1.2 Automatic Synchronization

This method similar to the manual technique, however it requires no human intervention. Instead, a synchronizer (device 25A) is employed to control the voltage, frequency, and phase angle. Then, it provides a correction signal for voltage and frequency matching to ensure a perfect synchronization [24]. Figure 4.3 shows the operation concept of an automatic synchronization.

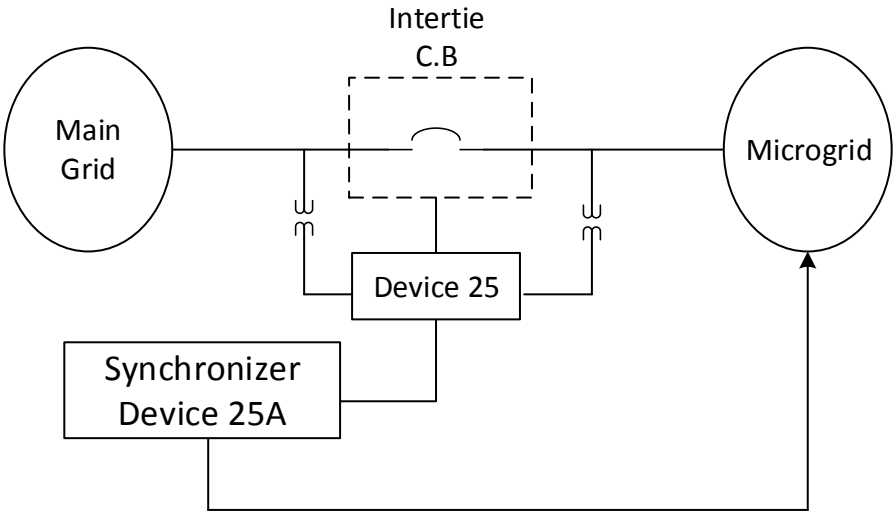

Figure 4.3 – Automatic Synchronization Diagram

4.1.1.2.1. PLL Based Automatic Synchronization

The phase locked loop (PLL) synchronizer is a common automatic synchronization method. The function of this type of synchronizer is to compare an entering signal to a reference signal. The output of the PLL is a corrected input signal where the output is synchronized with the reference input signal. When the two signals are almost identical in phase and magnitude, the synchronizer initiates a closing command. As pointed out in [25], a PLL for a balanced three phase system is commonly constructed using the direct and quadrature axis transformation (DQ axis). The three phase measured voltages at the PCC are transformed to a stationary two axis frame, and then to rotating reference frame by what is known as Park's transformation [9]. The following equations illustrate the sequences of moving from ABC axis to rotating DQ axis.

$$Va = V\ cos\omega t \tag{4.1}$$

$$Vb = V\ cos\omega t - \frac{2\pi}{3} \tag{4.2}$$

$$Vc = V\ cos\omega t + \frac{2\pi}{3} \tag{4.3}$$

$$\begin{pmatrix} Vd \\ Vq \end{pmatrix} = \frac{2}{3}\begin{pmatrix} cos\ \theta & \cos(\theta - \frac{2\pi}{3}) & \cos(\theta + \frac{2\pi}{3}) \\ \sin\theta & \sin(\theta - \frac{2\pi}{3}) & \sin(\theta + \frac{2\pi}{3}) \end{pmatrix}\begin{pmatrix} Va \\ Vb \\ Vc \end{pmatrix} \tag{4.4}$$

Where,

V: the peak amplitude voltage of the phasor

Vd: the direct axis voltage

Vq: the quadrature axis voltage

ω: the frequency of the phasor

θ: the angle of transformation, $\omega_0(t) + \Theta_0$ for synchronously rotating

In this study, PLL based automatic synchronization is used, however; there are other methods that accomplish the same goal.

4.2. Islanding Detection

Usually, microgrids are connected to the EPS to achieve a high level of efficiency. However, there are some situations where the EPS experiences conditions that require the microgrid to switch to a stand-alone mode. Therefore, when referring to islanding detection, it means, it is an unintentional case that has led the microgrid to be disconnected from the bulk power system. It is critical for a microgrid to distinguish between a normal and abnormal

situations to achieve satisfactory protection goals and protect human safety [26]. There are a number of causes that would lead the PCC breaker to initiate a disconnect function from the main grid, such as faults on the main system, power quality issues, frequency disturbances, and maintenance. It is important that the islanding detection recognize an unintentional islanding, otherwise the loss of mains would occur and the grid equipment, DGs, and the utility line crews may be in risk [27]. Figure 4.4 shows an islanded microgrid.

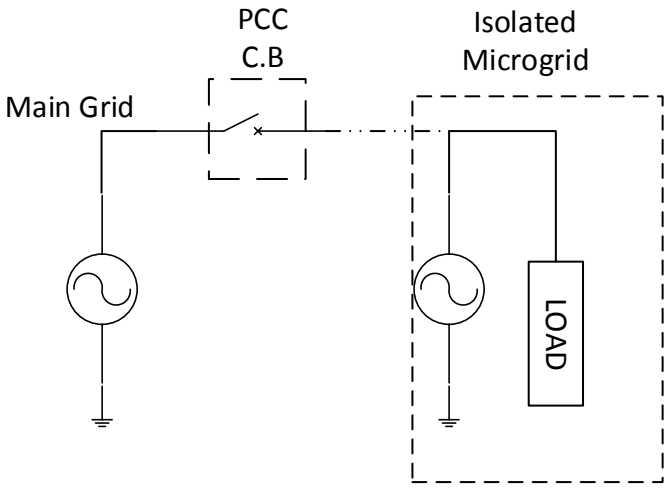

Figure 4.4 – Example of Islanded Microgrid

4.2.1 Islanding Detection Methods

Islanding detection methods can be categorized in three types: passive, active, and communication based [28], [29].

4.2.1.1. Passive Islanding Detection Methods

Passive detection methods work by measuring and monitoring some of the system quantities [26]. Then, set thresholds are compared with the system measured parameters.

When the parameters exceed the threshold continuously for a set time period, an islanding condition is confirmed. In order to avoid unwanted detection the threshold should be set properly. There are several techniques that apply passive islanding detection methods such as over/under frequency (OUF) or over/under voltage (OUV) detection, phase jump detection, and harmonic detection. This method can be applied to both inverter and synchronous machine based DG [26]. One of the disadvantages of passive islanding detection methods is that they can have problems in cases where load in the islanded system is nearly matched with DG output.

4.2.1.2. Active Islanding Detection Methods

Active detection methods are suitable for inverter based DG, with the basic concept of generating a disturbance using the output of the inverter. This disturbance would change at least one of the following parameters (frequency, voltage, real power, or reactive power) [26]. There will be a small change for those parameters during grid connected mode, and a larger change when islanded. Therefore, when an islanding condition occurs due to frequency or voltage drift for example, the case will be detected and isolation established. Active islanding detection methods include: frequency drift, voltage drift, and grid impedance estimation.

4.2.1.3. Communication Based Islanding Detection Methods

The communication method is very effective, but more expensive [29]. In this method a communication device sends a frequency signal to a receiver device close to the DG side to act according to the sent signal. During an abnormal condition, the DG would react to the sent signal and form an islanding microgrid. This method can be achieved by using the supervisory control and data acquisition SCADA system, power line carrier, and a dedicated line of

communication. Another way to detect an islanded condition is the status of the circuit breaker. If the breaker is open, the microgrid is disconnected from the grid side of the opened circuit breaker. A signal is then sent to the protection and control devices indicating that the breaker is open.

4.2.2 Islanding Detection Time

The islanding detection time in a system with synchronous machine based DG is determined according to the system's inertia constant for a certain power mismatch [29]. The time can be calculated as equation (4.5)

$$t = \frac{2\ \mathrm{H}\ \Delta f}{f \Delta P} \tag{4.5}$$

Where,

t: the islanding detection time (sec)

H: the machine inertia constant (sec)

Δf: the frequency deviation (Hz)

ΔP: the real power mismatch (W)

f: the nominal frequency (Hz)

A typical islanding detection time is between 200ms – 300ms [30]. For two DGs or more, the islanding detection time is related to the equivalent inertia for the multiple DGs. Reference [29] explains how the islanding detection time can be calculated for multiple machines. Equation (4.5) remains the same, however, the machine inertia constants will be for n machines. Equation (4.5) then, can be rewritten as equation (4.6) for machines.

$$t = \frac{2\,\mathrm{Heq}\,\Delta f}{f\Delta P} \tag{4.6}$$

$$H_{eq} = H_1\frac{Srated1}{Sbase} + H_2\frac{Srated2}{Sbase} + \ldots\ldots\ldots + H_n\frac{Sratedn}{Sbase} \tag{4.7}$$

Where,

H_{eq}: equivalent machines inertia constant

S_{rated1}: rated MVA of machine 1

S_{base}: base MVA

n: number of machines

4.2.3 Islanding Detection Requirements

There are a few basic requirements for islanding detection methods to avoid nuisance tripping or failures of detection:

1. Dependability: the devices should detect the islanding condition starting from all possible grid connected conditions.
2. Security: the schemes should be activated for the islanding condition and should ignore the other grid situations.
3. Selectivity: the islanding detection devices should distinguish between short disturbances in the power system such as conditions where upstream breakers trip and reclose and the requirements for islanding.

4.3. IEEE Standard and Considerations for Synchronization and Islanding Detection

The IEEE1547-2003 standard was issued to provide a guidance for connecting DRs with the EPS and specifies some requirements for the interconnection between two systems [18]. There are a series of standards for IEEE 1547 as below:

- 1547.1 IEEE Standard Conformance Test Procedures for Equipment Interconnecting Distributed Resources with Electric Power Systems [31].
- 1547.2 IEEE Application Guide for IEEE Std 1547, IEEE Standard for Interconnecting Distributed Resources with Electric Power Systems [32].
- 1547.3 IEEE Guide for Monitoring, Information Exchange, and Control of Distributed Resources Interconnected with Electric Power Systems [33].
- 1547.4 IEEE Guide for Design, Operation, and Integration of Distributed Resource Island Systems with Electric Power Systems [34].
- 1547.6 IEEE Recommended Practice for Interconnecting Distributed Resources with Electric Power Systems Distribution Secondary Networks [35].
- P1547.7/D11 IEEE Draft Guide to Conducting Distribution Impact Studies for Distributed Resource Interconnection [36].

For synchronization requirements, the standard states that "the DR unit shall parallel with the Area EPS without causing a voltage fluctuation at the PCC greater than ±5% of the prevailing voltage level of the Area EPS at the PCC, and meet the flicker requirements." Figure 4.5 shows the synchronization parameter limits for synchronous interconnection to an EPS.

Aggregate rating of DR units (kVA)	Frequency difference (Δf, Hz)	Voltage difference (ΔV, %)	Phase angle difference (ΔΦ, °)
0 – 500	0.3	10	20
> 500 – 1 500	0.2	5	15
> 1 500 – 10 000	0.1	3	10

Figure 4.5 - Synchronization Parameter Limits for Synchronous Interconnection to an EPS [32]

For unplanned islanding detection, the standard requires that “For an unintentional island in which the DR energizes a portion of the Area EPS through the PCC, the DR interconnection system shall detect the island and cease to energize the Area EPS within two seconds of the formation of an island” [32].

Chapter 5: Modeling the Studied City Microgrid

This chapter describes the constructed microgrid model in detail. The proposed microgrid is represented using an EMTP/ATP model that includes all the relevant control circuits. The ATP file includes different elements such as the power circuit, machine model, and the synchronization control models as well as the islanding detection scheme. The overall power circuit is implemented based on data from a Powerworld model has been created by another student.

5.1. Power System Model Description

The overall model is illustrated in Figure 5.1, where a microgrid, consisting of two DGs and four critical loads, is connected to the main power grid through four points of common coupling. The model built in ATP is shown in Figure 5.2 where the power circuit consists of six main parts: two generators, four transformers, four loads, three transmission lines, one capacitor bank, and four main PCCs connected to four different substations. The specifications of the different components are described in the following subsections.

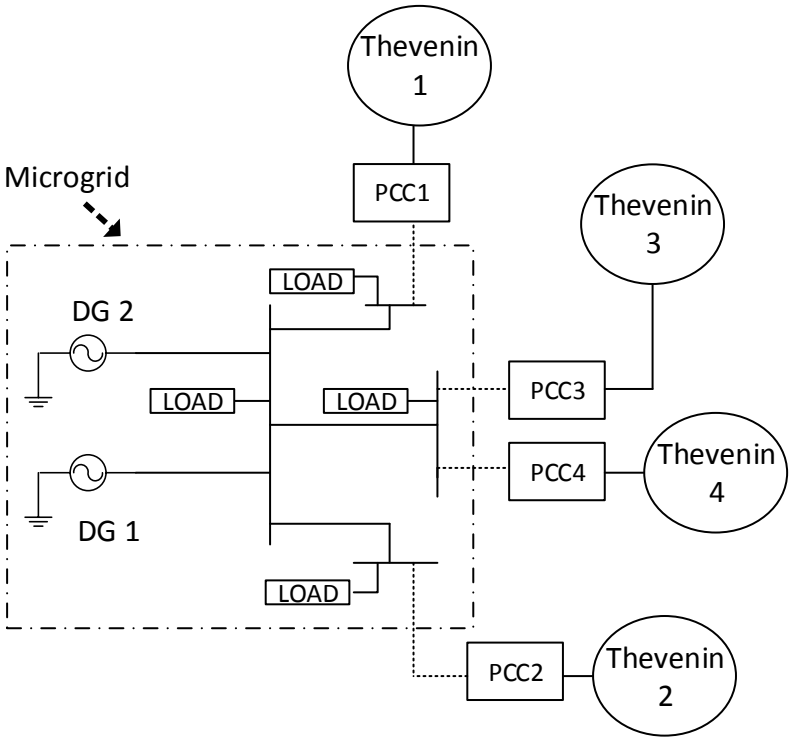

Figure 5.1 –Diagram of the Microgrid Studied in this Work

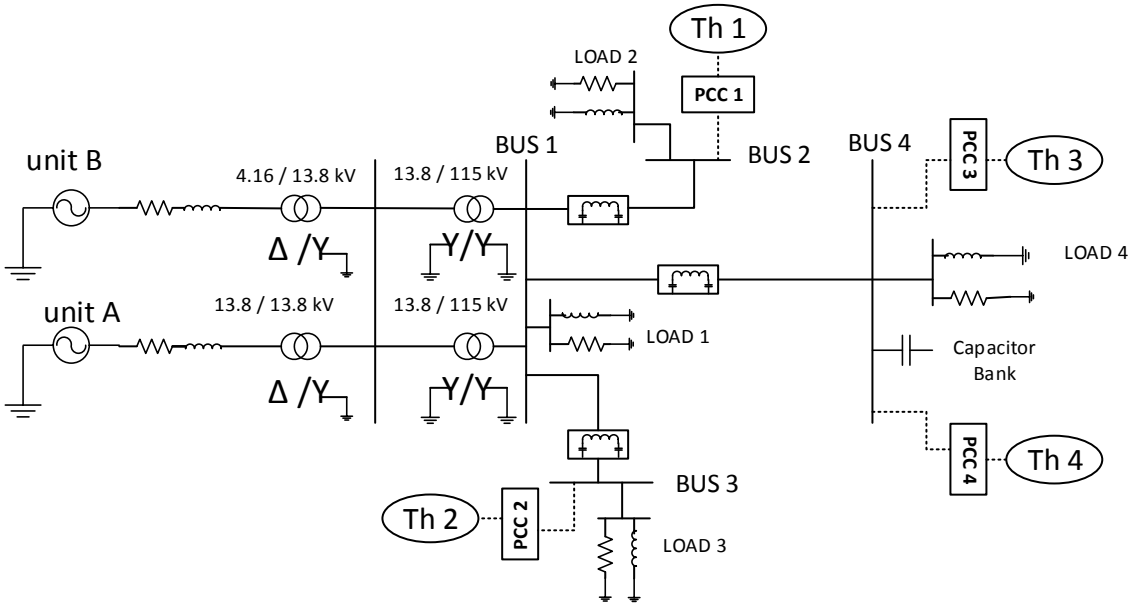

Figure 5.2 – Power System Model Implemented in ATP

Two Generators:

The generators modelled in this system are hydroelectric generators. The first unit (Unit A) is rated at 13.8 kV, 15 MVA and a smaller unit (Unit B) that is 4.16 kV, 10 MVA. Unit B is modelled in ATP as a type 60 TACS controlled source. Each phase is built as a separate controlled source to allow for better control over the power system. Additionally this allows for different tests and studies to be achieved on the generator side. Unlike unit B, unit A is built with more complex details. The unit model is described later in this chapter.

Four Substations:

The first substation connects the generator step up transformers to local network at Bus 1. The second substation is connected to the first PCC at Bus 2. Substation three is connected to PCC number 2 at Bus 3. The fourth substation has two connections to the main grid via PCC 3 and PCC 4 at bus 4.

Four Transformers:

All the transformers are modelled with 3 phases and 2 windings, using the general saturable transformer model in ATP. Three of these transformers are step up transformers, and the fourth one is an isolation transformer connected to unit A.

Three Transmission Lines:

Three 115 kV transmission lines connect substation 1 to the other three substations. All the transmission lines are modelled as 3-phase RLC coupled PI-equivalent models.

Four Loads:

The loads are modelled as parallel R-L loads connected to each substation. The loads are calculated according to the Powerworld model as constant real and reactive power.

Table 5.1: Microgrid Load Ratings during Grid Connected Operation

	Real Power (MW)	**Reactive power (MVAR)**
Load 1	23.7	7.19
Load 2	34.95	10.2
Load 3	17.32	8.64
Load 4	49.95	20.83

One Capacitor Bank:

A three phase delta connected capacitor bank is connected to substation number 4 and is rated at 91.6 MVAR.

Four Thevenin Sources Looking into Grid:

During grid connected mode, each PCC is connected to a Thevenin source that represents the main grid. In order to calculate the Thevenin voltage source and impedance, a short circuit test was done at each PCC in Powerworld while disconnecting the microgrid from the main grid.

Table 5.2: Calculated Thevenin Voltages and Impedances

	V_{thev} (kV)	Z_{thev} (Ω)
Thevenin 1	115.805 at 71.67 deg	1.85 + j 7.881
Thevenin 2	115.45 at 70.06 deg	1.38 + j 4.947
Thevenin 3	115.39 at 71.39 deg	0.602 + j 2.959
Thevenin 4	115.21 at 71.08 deg	0.672 + j 2.925

5.1.1. Power System Model Validation

The ATP model has been validated using two different programs: Powerworld and Mathcad. Short circuit tests were done in different locations in the power system to observe the variations between the models. The validation results show a comparable match between the three programs with less than 5% error.

5.2. Unit A Machine Model

Unit A is considered as the master DG in this particular microgrid, therefore a more detailed machine model has been used for this unit to obtain results with higher precision. According to the project sponsor, unit A used to have both an exciter and governor. At some point, the governor was removed. In the ATP file, a type 59 synchronous machine is used to model the unit A hydroelectric machine. The type 59 machine allows two external inputs: the field voltage that is obtained from the exciter, and the mechanical power that would come from the prime mover as controlled by the governor control circuit. The other machine

parameters are entered into the machine directly. Unit A machine parameters are given in Appendix B. Figure 5.3 shows the unit A machine diagram.

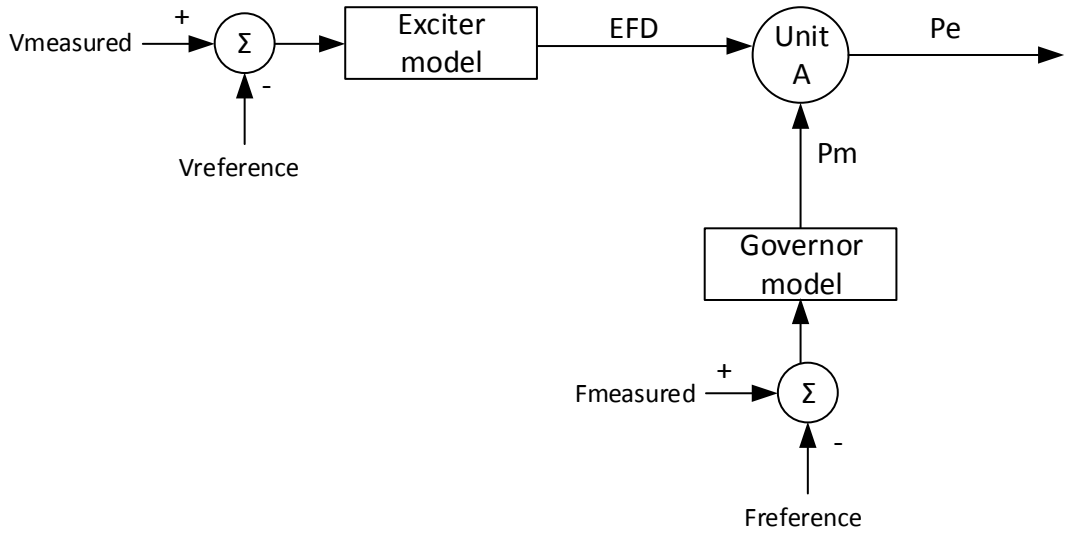

Figure 5.3. – Unit A Machine

Where,

$V_{measured}$: the machine terminal voltage

$F_{measured}$: the system's frequency

EFD: the exciter field voltage

P_m: the mechanical power

P_e: the electrical power out of the machine

5.2.1 Unit A Exciter Model

The exciter is represented using a static excitation system with the standard ST4B model. The voltage regulator of this model is typically implemented digitally as indicated by the letter B used in the model name [37].

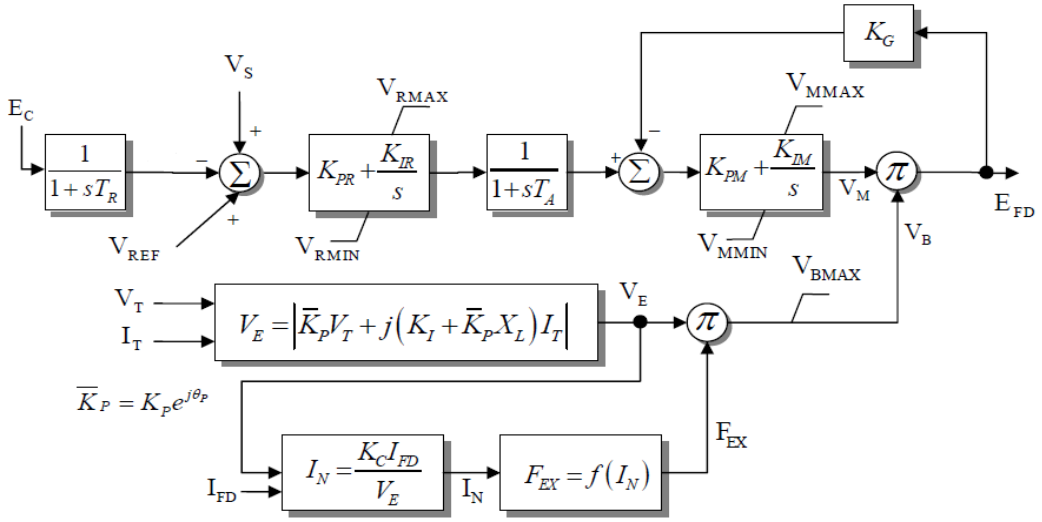

Figure 5.4. – Type ST4B Potential or Compound Source Controlled Rectifier Exciter [37].

Where,

T_R: Filter time constant (sec)

K_{PR}: Voltage regulator propotional gain (pu)

K_{IR}: Voltage regulator integral gain (pu)

V_{RMAX}: Maximum voltage regulator output (pu)

V_{RMIN}: Minimum voltage regulator output (pu)

T_A: Voltage regulator time constant (sec)

K_{PM}:Voltage regulator proportional gain output (pu)

K_{IM}: Voltage regulator integral gain output (pu)

V_{MMAX}: Maximum inner loop output (pu)

V_{MMIN}: Minimum inner loop output (pu)

K_G: Feedback gain constant of the inner loop field regulator (pu)

K_P: Potential circuit gain coefficient (pu)

K_I: Potential circuit gain coefficient (pu)

V_{BMAX}: Maximum excitation voltage (pu)

K_C: Rectifier loading factor proportional to commutating reactance (pu)

X_L: Reactance associated with potential source (pu)

V_T: The bus voltage (pu)

I_T: The stator current (pu)

E_C: Votage compensator (pu)

V_S: Output terminal voltage (pu)

I_{FD}: Field current (pu)

E_{FD}: Field voltage (pu)

5.2.2 Unit A Governor Model

A governor was added to the system since the machine lacks a governor, and one will be needed for the microgrid. The governor model is based on the IEEE standard hydro turbine governor model HYGOV [38].

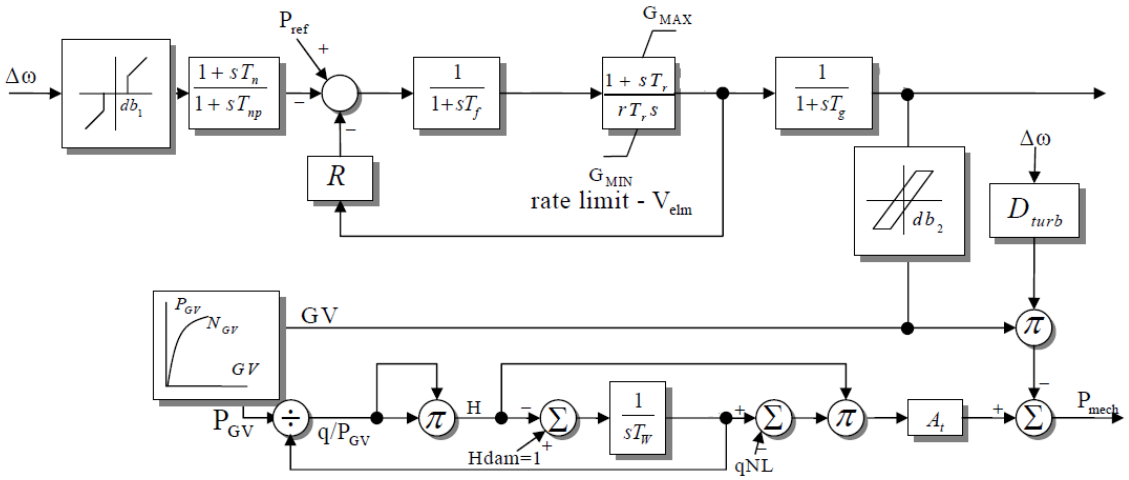

Figure 5.5. – Type HYGOV Governor Model [38],[39].

Where,

P_{mech}: Mechanical output power (pu)

Δ_{ω}: The rate of change of speed (pu)

db_1: Intentional deadband width (pu)

T_p: Pilot servo time constant (sec)

db_2: Unintentional dead-band (pu)

R: Permanent droop (pu)

r: Temporary droop (pu)

T_r: Governor time constant (sec)

D_{turb}:Turbine damping factor (pu)

H_{DAM}: Head available at dam (pu)

T_W: Water inertia time constant (sec)

q_{NL}: No-load flow at nominal head (pu)

A_T: Turbine gain (pu)

T_r: Washout time constant (sec)

T_f: Filter time constant (sec)

T_g: Gate servo time constant (sec)

V_{ELM}: Maximum gate velocity (pu)

G_{MAX}: Maximum gate opening (pu)

G_{MIN}: Minimum gate opening (pu)

5.3. Modeling the Synchronization Circuit (PLL- control circuit) for Unit A and Across the PCCs

The system frequency is tracked using a PLL control circuit. Figure 5.6 shows the basic schamatic diagram of the synchronization signal process. The system's three phase voltages at the opposite sides of a PCC or unit A breaker are transformed to rotating (synchronous) reference frame quantities (Vd, Vq). The transformations are made based on

the Park's transformation method. The quadrature voltage is entered to a proportional and integral PI controller, which is then added to the base system frequency. After that, a frequency limiter block is placed followed by a controlled integrator with a reset to get the reference angle that ranges between 0 to 2π. The reference angle (ϴR) is compared to the angle of the voltage entered to the PLL. To ensure a good system tracking, the difference between the two angles should be close to zero [9].

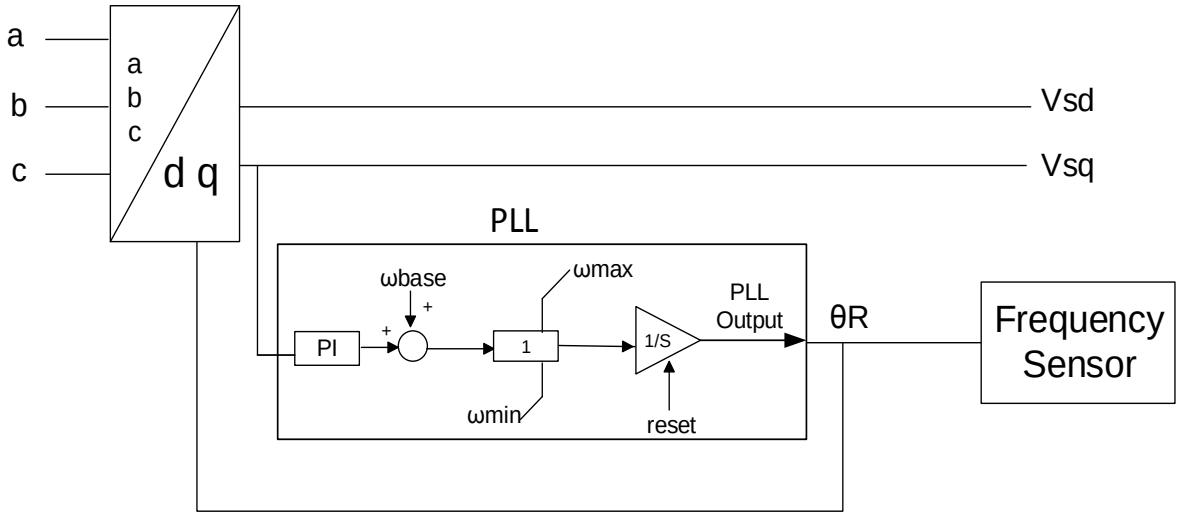

Figure 5.6. – Frequency Measurement Procedure Based on PLL

Where,

PI: the propotional and integral gains (pu)

ω_{base}: the base frequency in rad/sec

reset: a reset function whose output is reset to zero whenever it reaches 2π.

5.4. Islanding Detection Scheme

In this thesis, the DGs that are used to supply the microgrid are synchronous machine based hydro units; therefore, the islanding detection scheme is built based on a passive islanding detection method that monitors the voltages and frequencies at each PCC. This method is sutable for synchronous machine based DGs [29]. Similar to the over/under voltage and over/under frequency protection schemes and the rate of change of frequency (ROCOF) scheme, the proposed scheme is located at each PCC and measures the voltage and frequency across each PCC. The function of the OUV is implemented as shown in Figure 5.7 and the over/under frequency scheme is in Figure 5.8. During grid connected mode, the voltage and frequency at the grid side are measured and compared to the maximum and minimum allowable limits – as specified by IEEE 1547. If the EPS experiences an abnormal condition, the scheme in Figure 5.9 would detect the case and form a microgrid. The counters in Figures 5.7 and 5.8 represent the requirements for the OUV and OUF condition to stay true for a qualifying time before action is taken. The qualifying time is set longer than the trip reclose cycles for fault response or a stable swing.

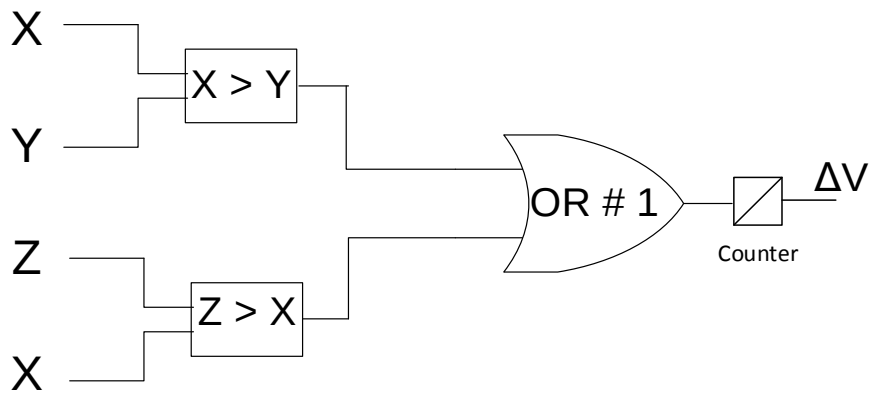

Figure 5.7. – OUV Detection Logic

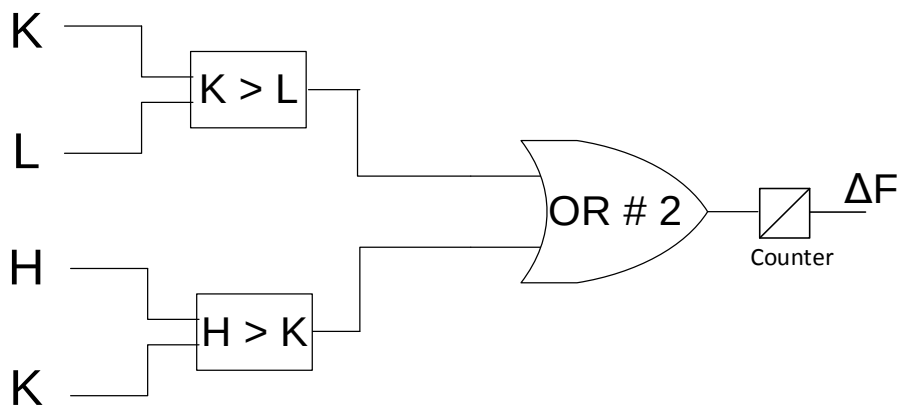

Figure 5.8. – OUF Detection Logic

Where,

X: The measured voltage magnitude at the PCC (pu)

Y: The maximum allowed voltage (1.1 pu)

Z: The minimum allowed voltage (0.88 pu)

ΔV: over/under voltage status – normally zero (pu)

K: The measured frequency (pu)

L: The maximum allowed frequency (60.5 Hz)

H: The minimum allowed frequency (59.3 Hz)

ΔF: over/under frequency status – normally zero (pu)

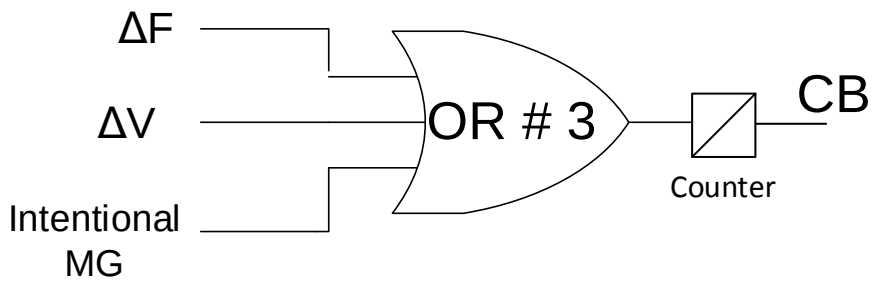

Figure 5.9. – PCC CB Trip Logic

- The third input on Figure 5.9 is for a manual command to form an intentional operation of microgrid.
- The counter in Figure 5.9 implements a requirement that the output be high for three consecutive sampling periods to qualify the output.

5.5. Building the Communication between the Master DG and the EPS

The communications between the master DG in the microgrid (unit A) and the PCC are modeled based on SCADA cycle delay of 10ms. The PCC frequency measurement is entered into a delay function that is used to imitate the SCADA system function. The delay is chosen to be 10 msec. The delayed signal is fed back to the unit A frequency model as shown in Figure 5.11.

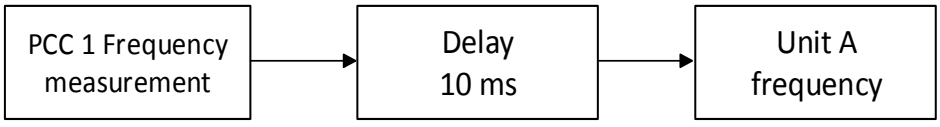

Figure 5.10: The Delay Function Implementation

The next chapter discusses the tests on the built models and shows the system responses during multiple system conditions.

Chapter 6: Simulation Tests Results

This chapter presents the ATP simulation procedure and results for the built microgrid. The results show the interaction and response of the main grid with the microgrid under multiple scenarios. The observed results are analyzed and disscussed after each case.

6.1. Simulation Test Procedure

The grid-connected and islanding operation modes of the microgrid are tested under three cases. In the first case, the models are tested during normal operation to illustrate the systems' response during normal conditions. Second, the system response is examined under fault events. A SLG fault is applied in the microgrid and the main grid in different locations in Figure 6.1, and the consequenses are monitored. Third, the system is simulated and tested during frequency swing conditions to show the response under this case.

In each tested case, the response of four of the models discussed in Chapter 5 are evaluated. The four discussed points are as follows:

1- The terminal voltage of unit A machine

2- The frequency tracking by the PLL control circuit

3- The OUV sceheme response

4- The OUF sceheme response.

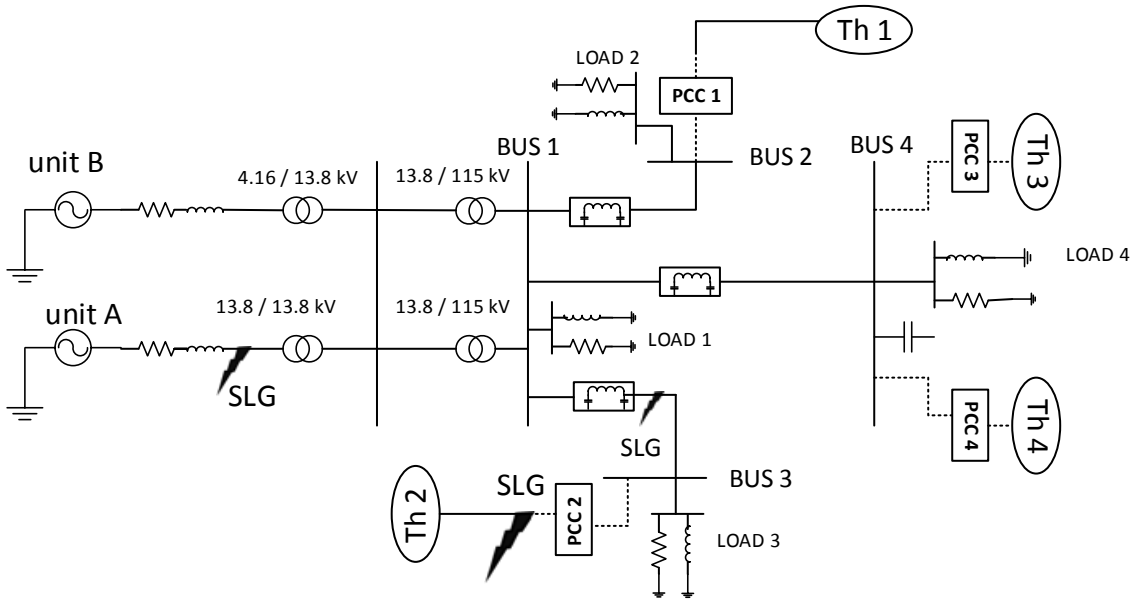

Figure 6.1: SLG Fault Locations

6.2. Case A – Grid Connected Simulation Results

In this test, results are obtained when the microgrid is connected to the main grid. Only PCC2 measurements are presented while the other PCCs will be discussed later on.

6.2.1. Event A.1 - Normal Condition

Normal condition means that the system is simulated during steady state conditions, with no fault is applied, nor is there any change in the system. The total load of the microgrid during grid connected is 125.92 MW and 46.8 MVAR is specified in Table 5.1.

6.2.1.1 Unit A Terminal Voltage

Since Unit A is a complex model, the terminal voltage of the unit is monitored for each case to ensure that the machine is working properly. Figure 6.2 shows that the terminal voltage is as expected (almost 11.26 kV) peak line to ground.

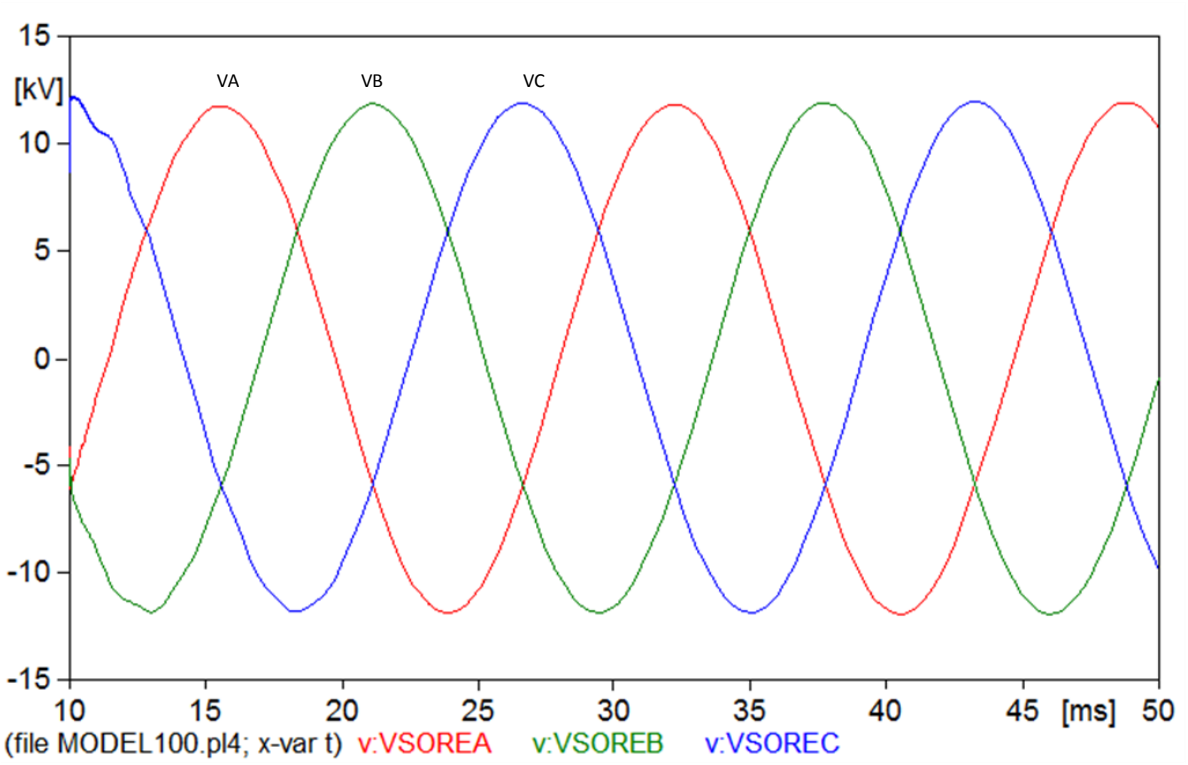

Figure 6.2: Unit A Terminal Voltage – Normal Condition – Grid Connected

6.2.1.2 PLL Frequency Tracking

The stationary and rotating reference voltages from the PLL are shown in Figure 6.3. To ensure that the PLL is correctly tracking the system frequency, the direct axis of the rotating reference frame voltage should look as a constant quantity that tracks the peak of the phase A voltage waveform. The quadrature axis of the rotating reference frame voltage should be zero. Vd will be constant if the power system is in steady state at the frequency of the transformation in equation (4.4). In this case, Figure 6.3 shows a perfect frequency tracking as expected based on PCC2 voltage measurements.

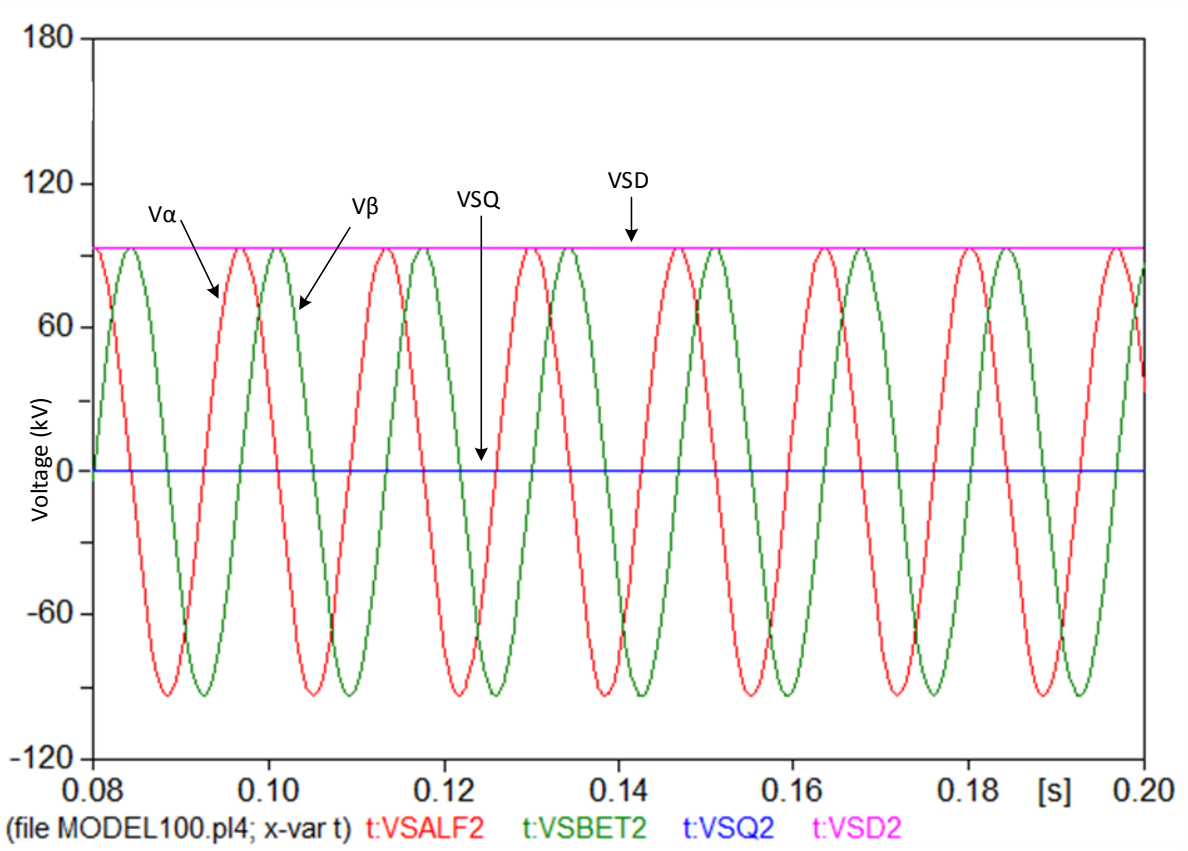

Figure 6.3: Frequency Tracking – Normal Condition – Grid Connected

In all the PLL Figures,

Vα (red): the staionary reference frame voltage at PCC2

Vβ (green): the staionary reference frame voltage that is shifted by 90 degrees at PCC2

VSQ (blue): the quadrature axis of the rotating reference frame voltage at PCC2

VSD (pink): the direct axis of the rotating reference frame voltage at PCC2

6.2.1.3 OUV Scheme

This test examines compliance with the IEEE 1547 requirements for the voltage in both the grid and microgrid sides. The OUV scheme is used to check the voltages. The

voltages should be within the maximum and minimum limits. Here, the maximum voltage is set at 1.1 pu, and the minimum voltage is set at 0.88 pu. Figures 6.4 and 6.5 shows that the requirements are maintained under normal conditions.

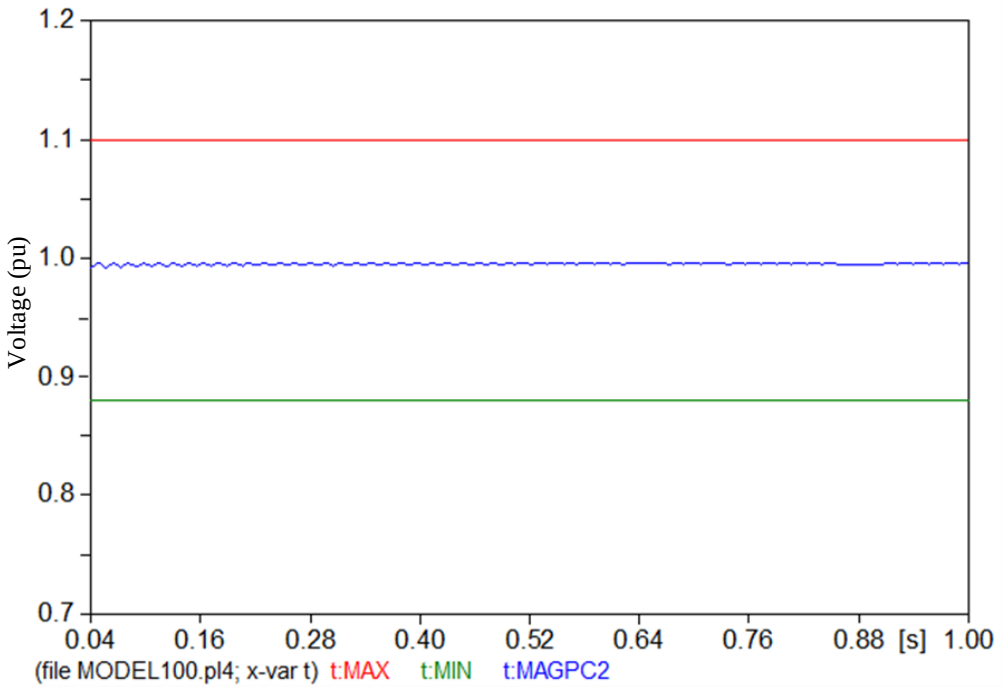

Figure 6.4: Voltage Level – Grid side – Normal Condition – Grid Connected

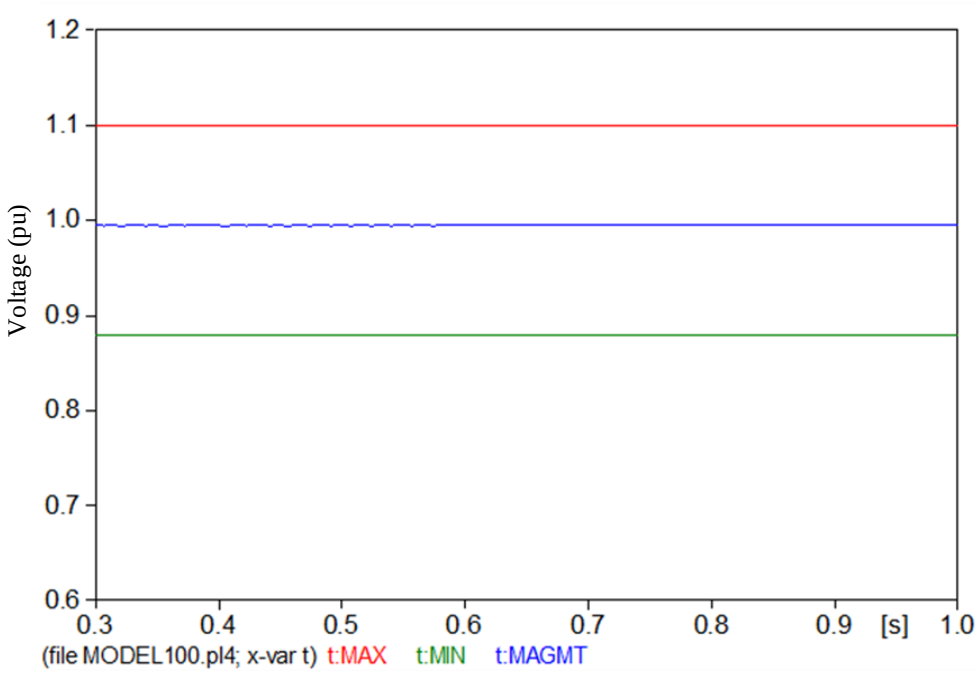

Figure 6.5: Voltage Level – Microgrid Side – Normal Condition – Grid Connected

6.2.1.4 OUF Scheme

This test examines the IEEE 1547 requirements for the frequency in both the grid and microgrid sides. The OUF scheme is used to check the frequency. The frequency should be within the maximum and minimum limits. Here, the maximum frequency is set at 60.5 Hz, and the minimum frequency is set at 59.3 Hz as per the standard. Figures 6.6 and 6.7 shows that the requirements are maintained under normal conditions.

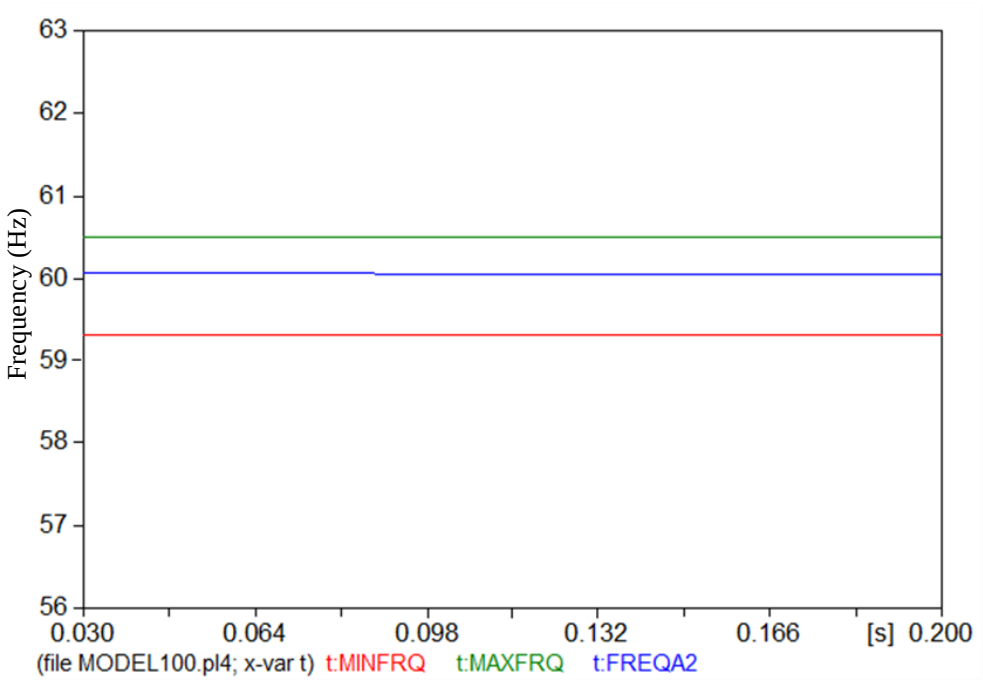

Figure 6.6: Frequency Level – Grid Side – Normal Condition – Grid Connected

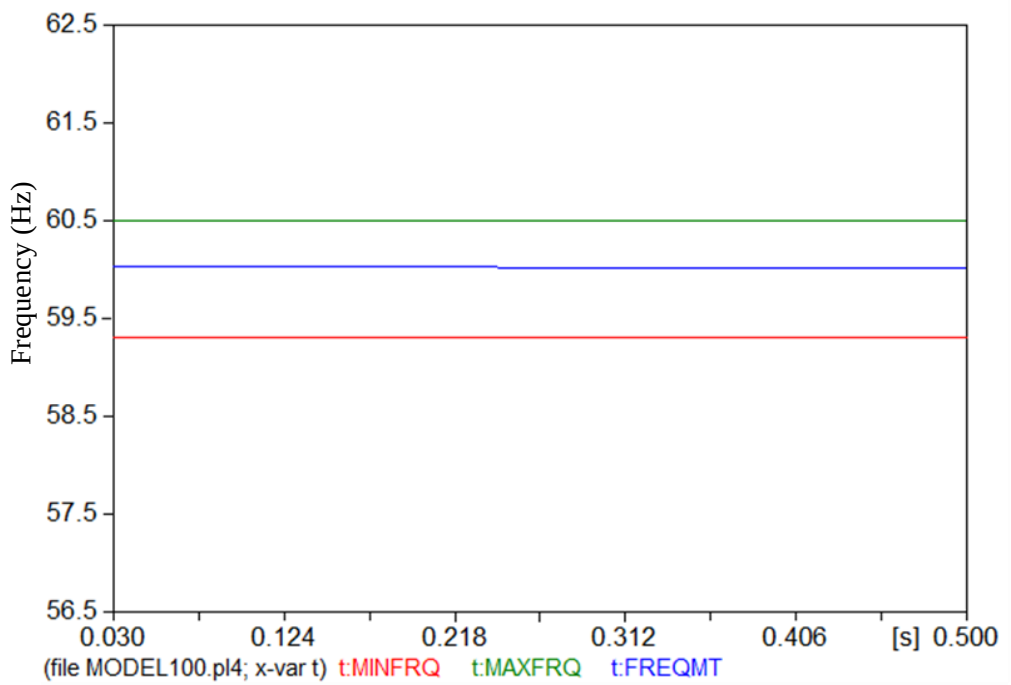

Figure 6 .7: Frequency Level – Microgrid Side – Normal Condition – Grid Connected

6.2.2. Event A.2 – SLG Fault

In this event, the system is tested under an abnormal condition. A SLG fault is applied to the grid side of PCC2 as shown in Figure 6.1. The fault is applied at 0.05s and cleared at 0.2s. The OUV and OUF tested under this case to ensure that they work properly.

6.2.2.1 Unit A Terminal Voltage

During SLG fault, unit A terminal voltage is effected and experiences unbalanced voltage as shown in Figure 6.8. The phase A voltage is below 11.26 kV during the fault and phases B and C experience overvoltage.

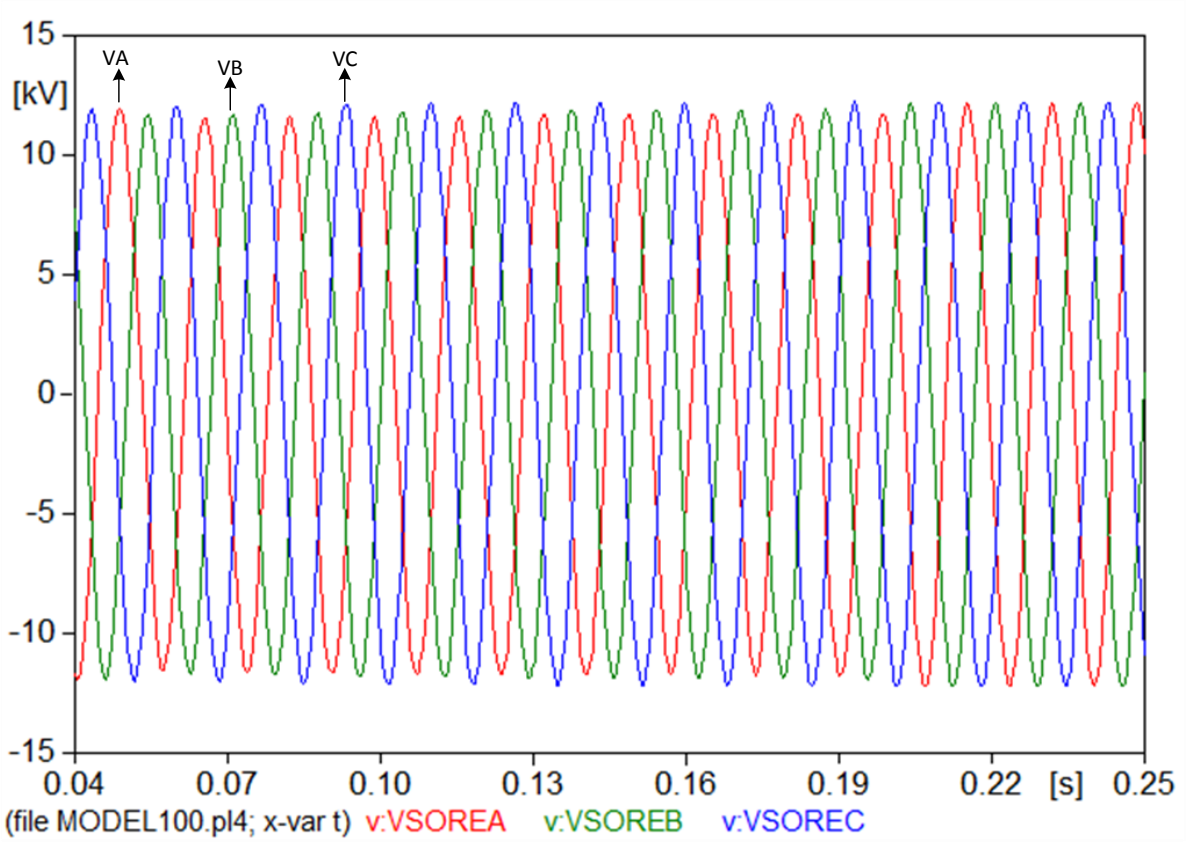

Figure 6.8: Unit A Terminal Voltage – SLG Fault Condition – Grid Connected

6.2.2.2 PLL Frequency Tracking

Even though the system experences a SLG fault, the frequency is tracked very well based on PCC2 voltage measurements. as shown in Figure 6.9. The PLL function at the PCC is not affected by the fault. The voltage sag due to the fault is captured in the direct axis voltage magnitude. The second harmonic due to the negative sequence voltage was removed with a filter (Apendix B provides more details).

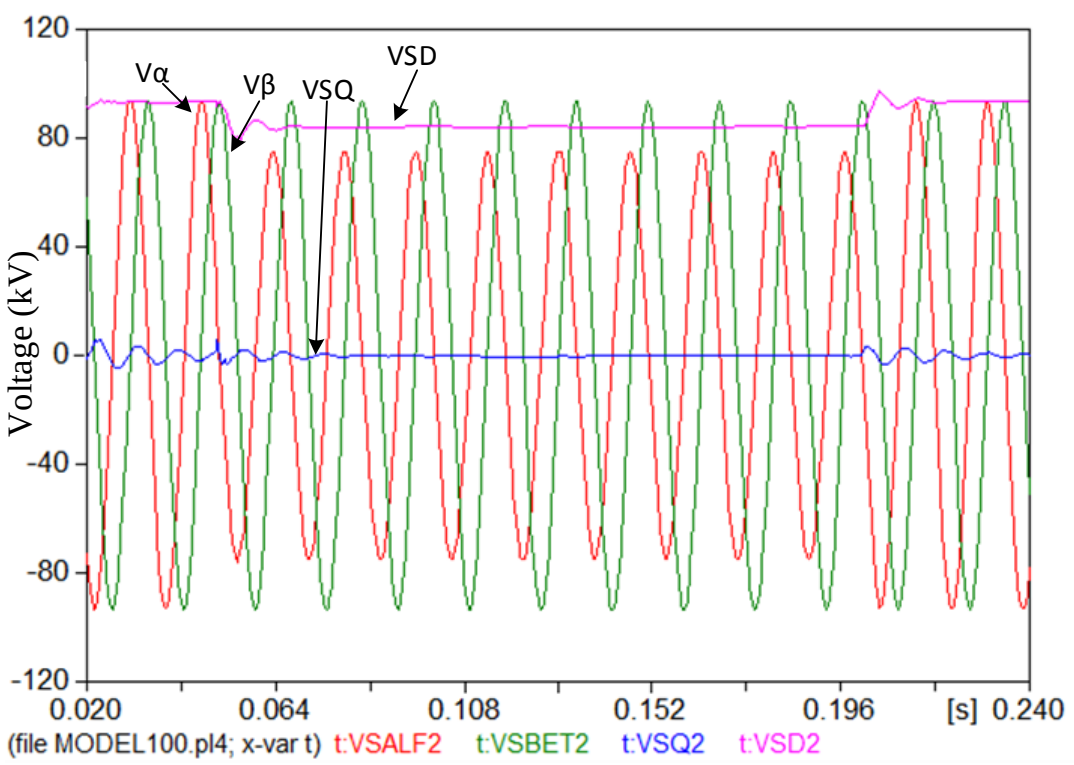

Figure 6.9: Frequency Tracking – SLG Fault Condition – Grid Connected

6.2.2.3 OUV Scheme

Figures 6.10 and 6.11 show that under a SLG fault while grid connected, the OUV scheme is not triggered and the relay does not pick up. On both sides (the main grid and the

microgrid), the measured voltages are within the limits. However, there is a transient behavior at the beginning of the faut this transient falls below the minimum threshold, but the counter function will detect this case and prevent false tripping.

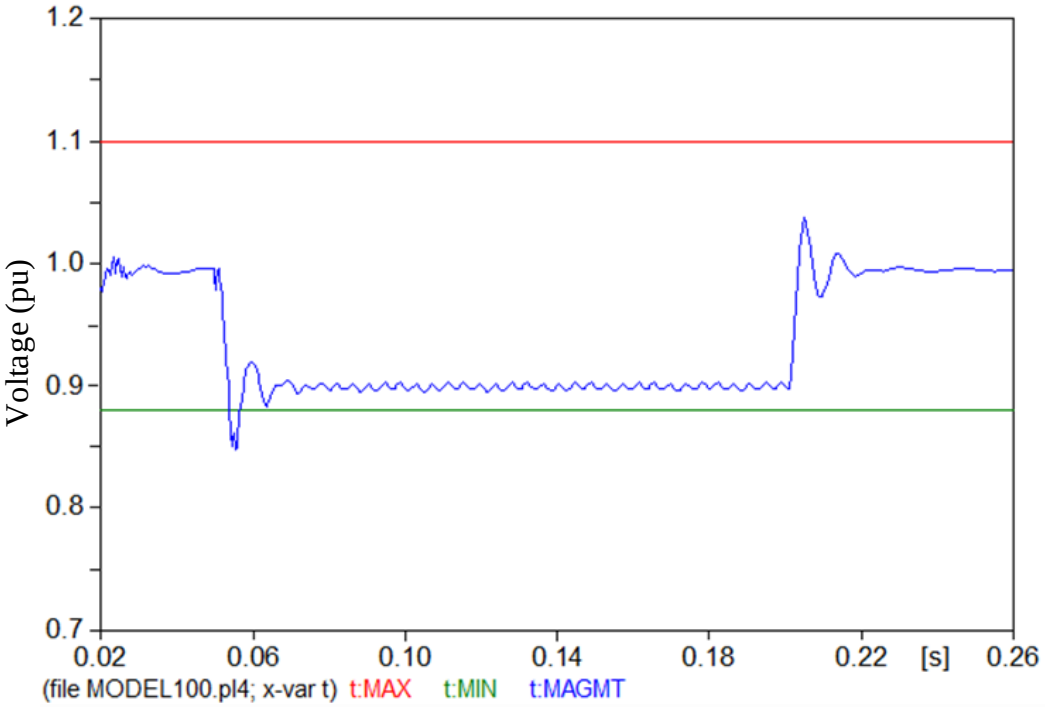

Figure 6.10: Voltage Level – Grid side – SLG Fault Condition – Grid Connected

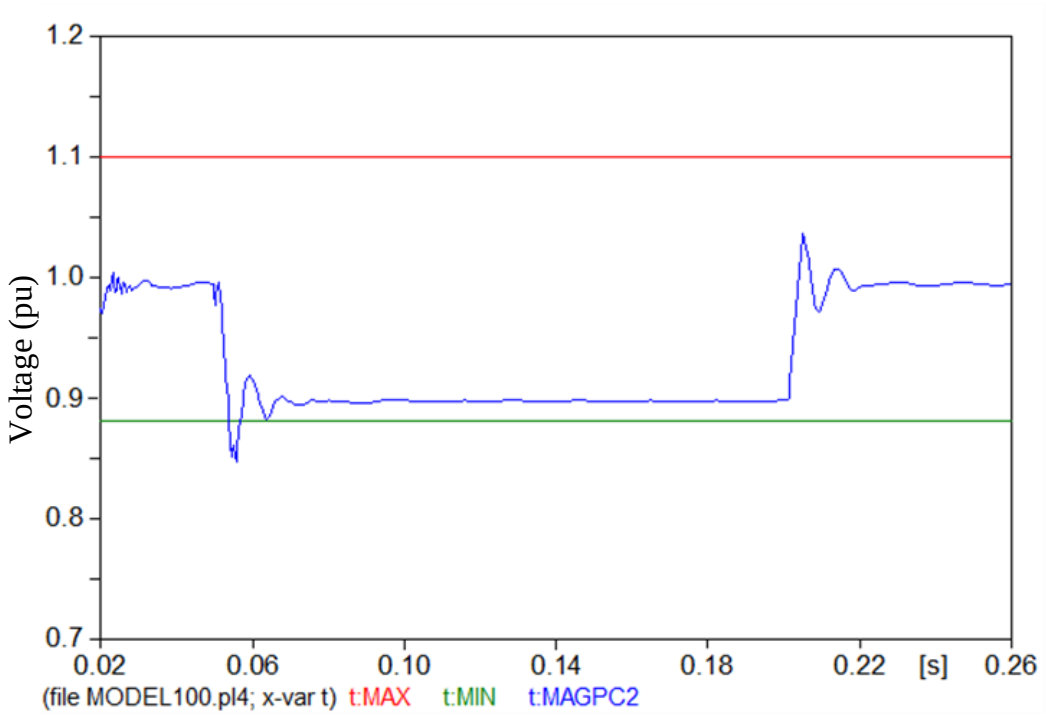

Figure 6.11: Voltage Level – Microgrid side – SLG Fault Condition – Grid Connected

6.2.2.4 OUF Scheme

Similar to the OUV, the OUF scheme does not pick up during the SLG fault when grid connected. Figures 6.12 – 6.13 show that the frequency within the limits in both the grid and microgrid sides.

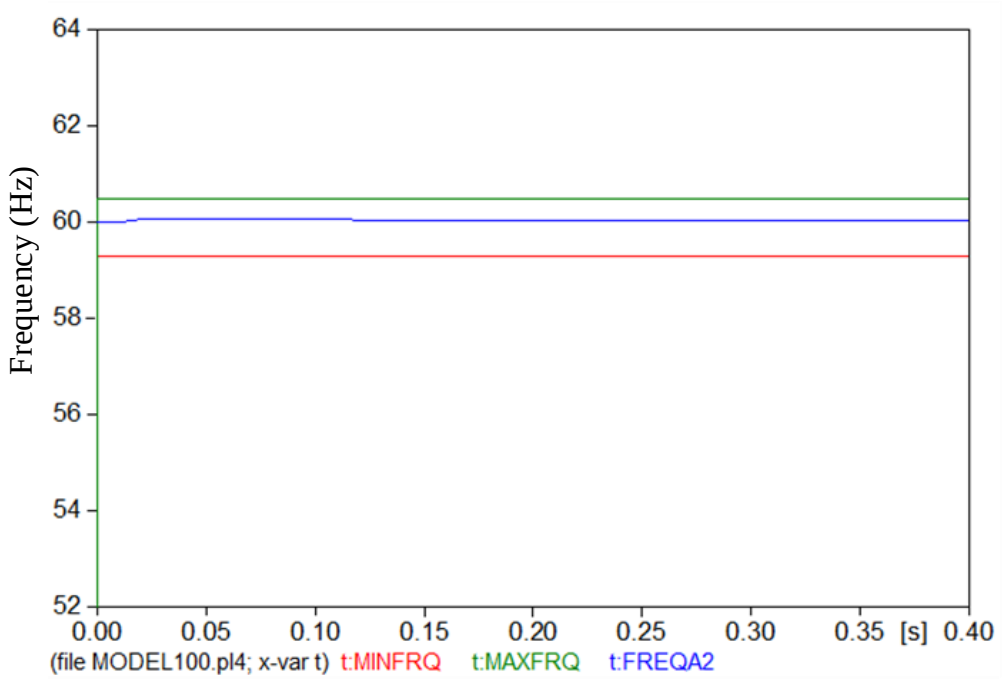

Figure 6.12: Frequency Level – Grid Side – SLG Fault Condition – Grid Connected

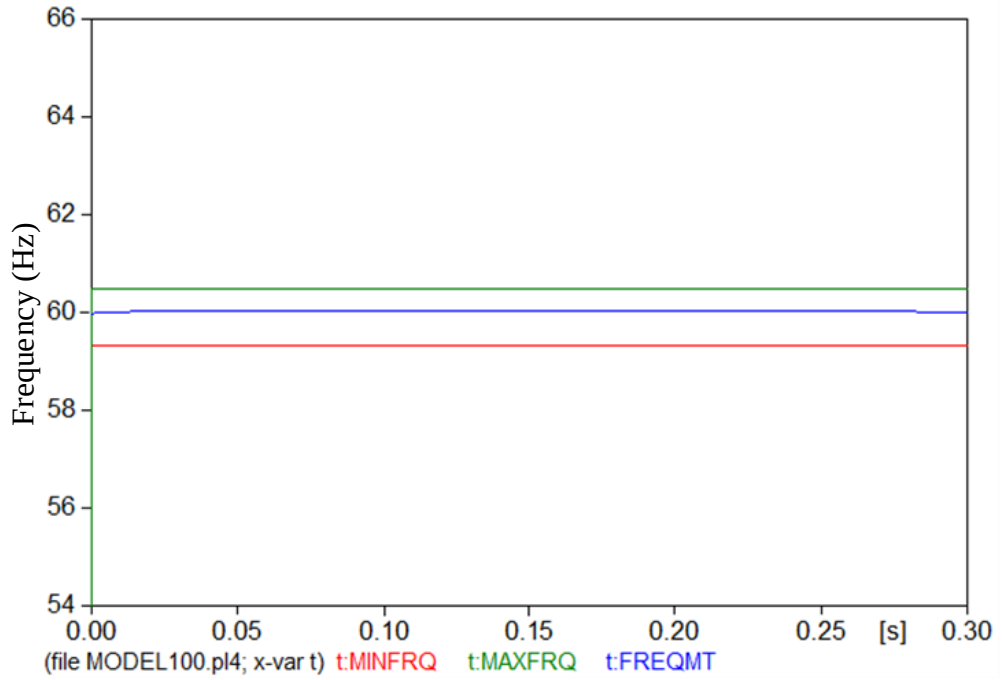

Figure 6.13: Frequency Level – Microgrid Side – SLG Fault Condition – Grid Connected

6.2.3. Event A.3 – Frequency Swing Condition (FSC)

In this test, the frequency at the four Thevenin sources as well as unit B source in Figure 6.2 experience a low frequency variation as could be seen during a power swing. The low frequency is 0.5 Hz and combined to the system frequency (60 Hz) as shown in equation (6.1). In order to represent how the low frequency is combined to the system's frequency, equation (4.1) is rewritten as:

$$Va = V\cos(\omega_1 t * \cos(\omega_2 t)) \quad (6.1)$$

Where,

$$\omega_1 = 2\pi\ 60\text{Hz}\ \ (\text{rad/sec}) \quad (6.2)$$

$$\omega_2 = 2\pi\ 0.5\text{Hz}\ \ (\text{rad/sec}) \quad (6.3)$$

Figure 6.13 shows the voltage at PCC 2 during the frequency swing condition. The response of the system and controls due to the frequency swing are illustrated in the following subsections.

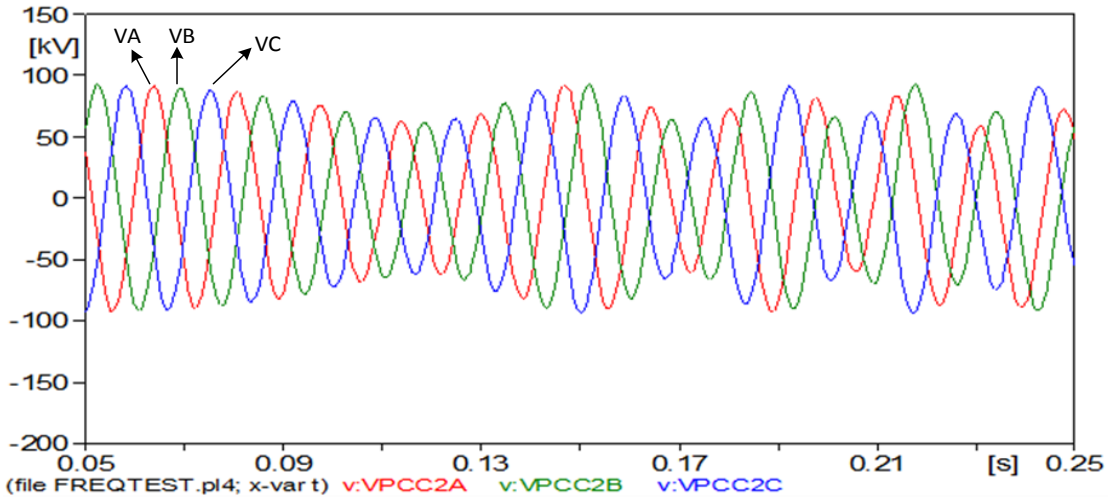

Figure 6.14: PCC 2 Voltage – Grid Side – FSC Test

6.2.3.1 Unit A Terminal Voltage

The terminal voltage of unit A experiences an unbalanced condition due to the frequency swing. While all five sources experience the frequency swing condition, the unit A machine acts properly and track the frequency change in the system as shown in Figure 6.15 which shows similar behavior as Figure 6.14.

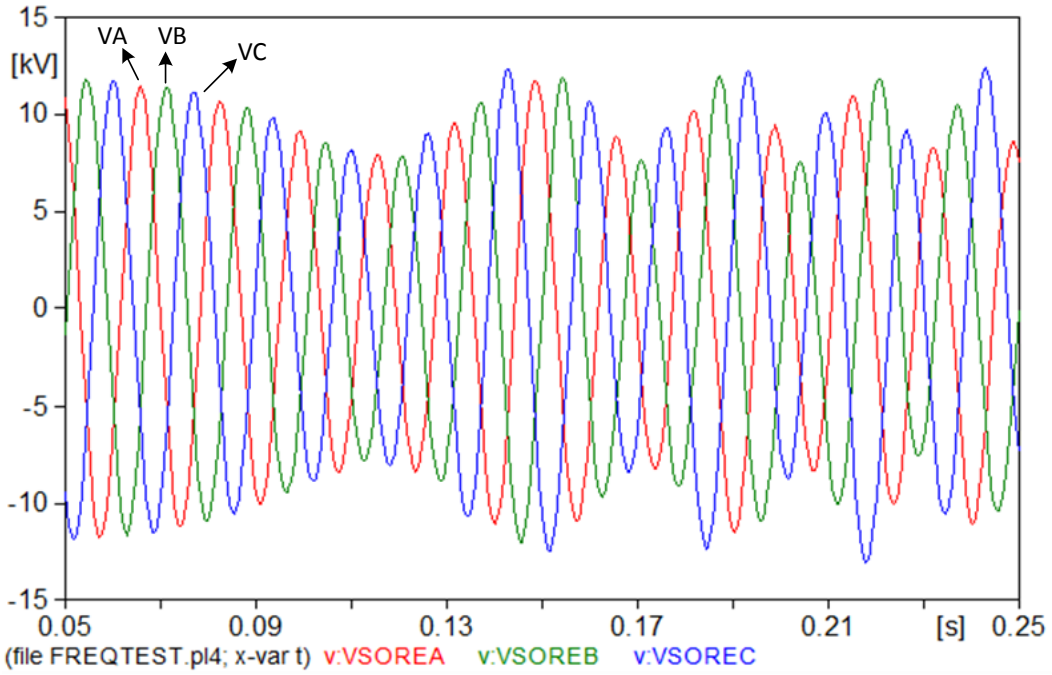

Figure 6.15: Unit A Terminal Voltage – FSC Test

6.2.3.2 PLL Frequency Tracking

During the FSC test, the frequency is not constant and the PLL output did not track the change as shown in Figure 6.16.

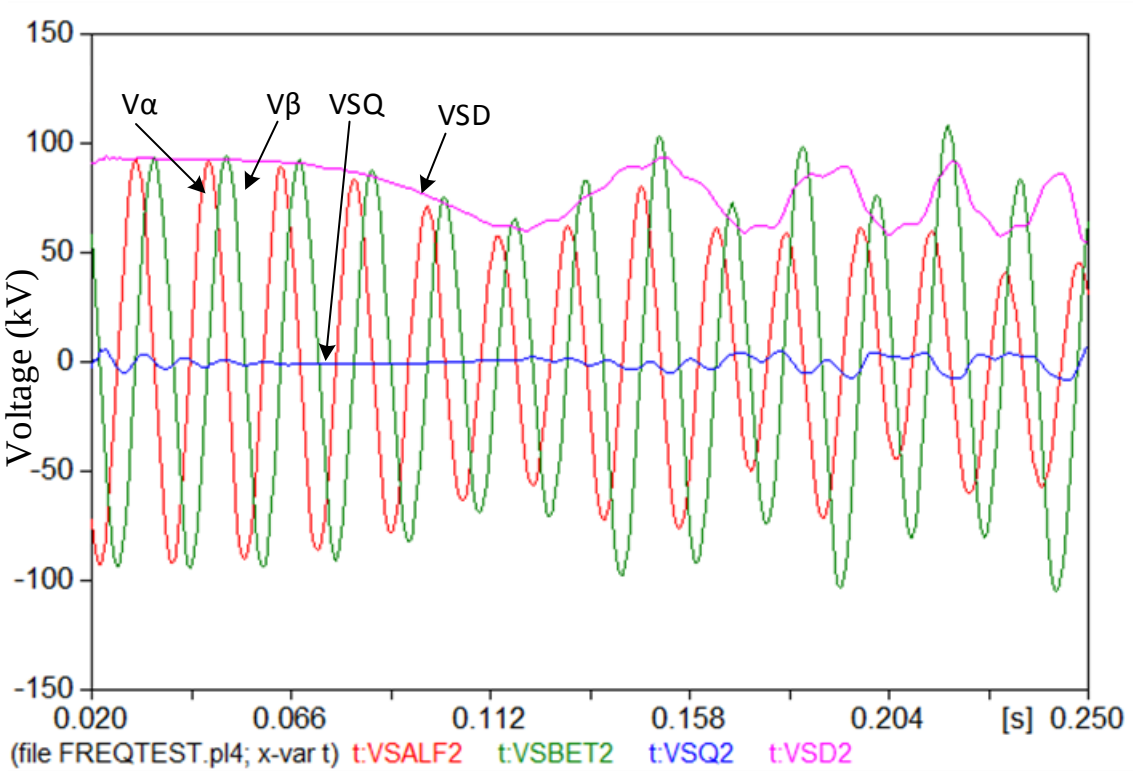

Figure 6.16: Frequency Tracking – FSC Test

6.2.3.3 OUV Scheme

During FSC, the voltages at the grid and microgrid sides are out of the allowable range (below 0.88 pu). Figures 6.17 and 6.18 show that the OUV scheme detects an under voltage condition due to the frequency error passing through the voltage measurements. Figures 6.17 and 6.18 show that the average value of the voltage waveform is about 0.65 pu

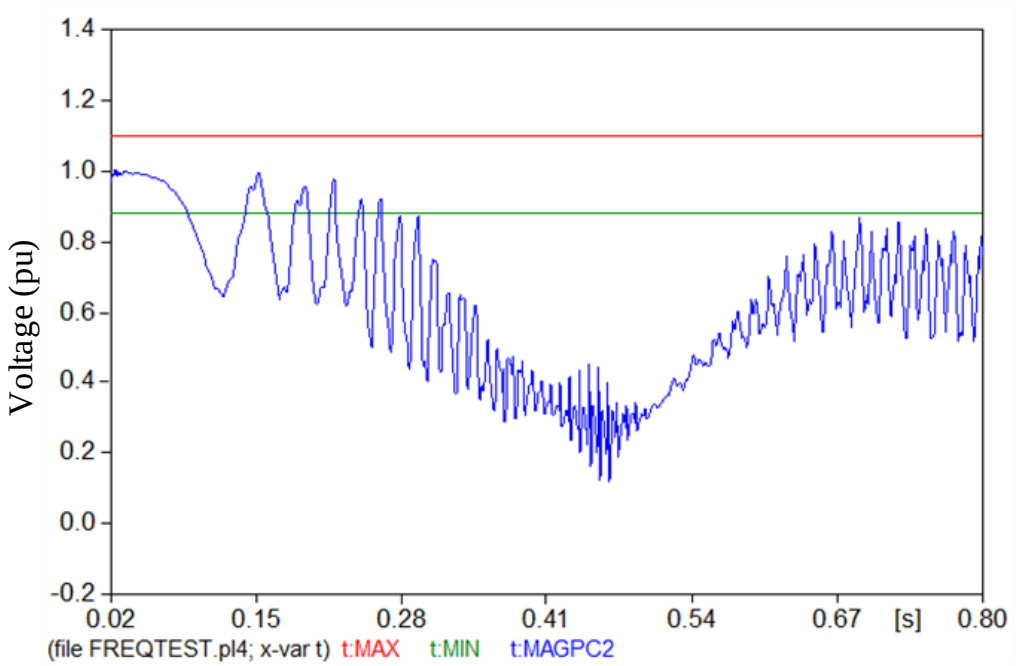

Figure 6.17: Voltage Level – Grid side – FSC Test

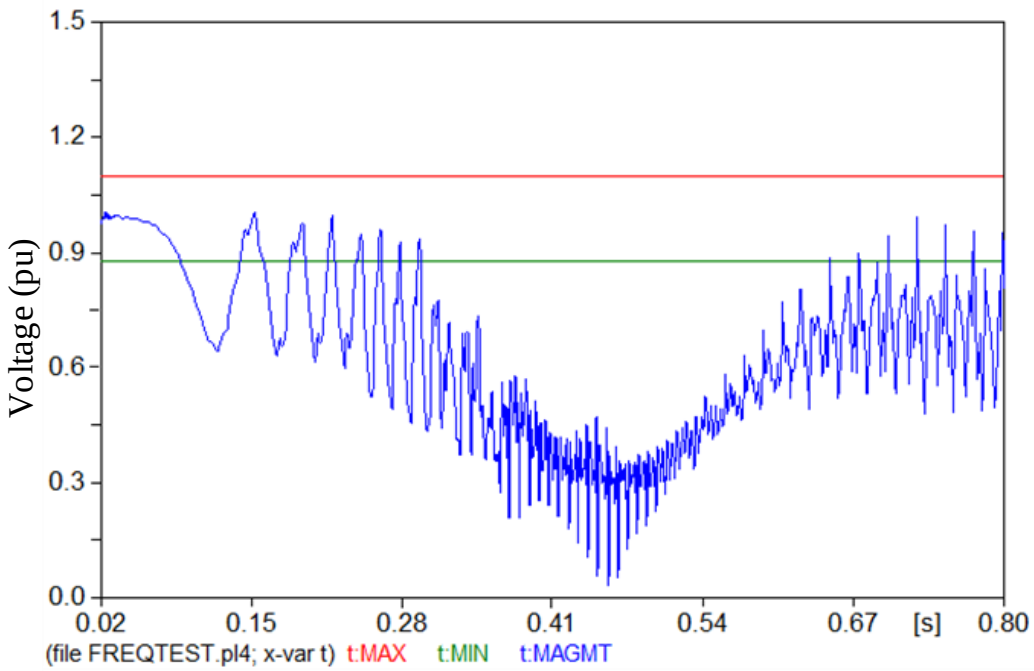

Figure 6.18: Voltage Level – Microgrid side – FSC Test

6.2.3.4 OUF Scheme

The OUF at the grid side is effected by the FSC. Figures 6.19 reveals that the frequency at the grid side of PCC 2 hits the frequency threshold for a short time. This means that the OUF scheme is activated, but will not trip due to the short time of violation (about 300 ms). However, the frequency at the microgrid side during FSC is within the accepted limits as shown in Figure 6.20.

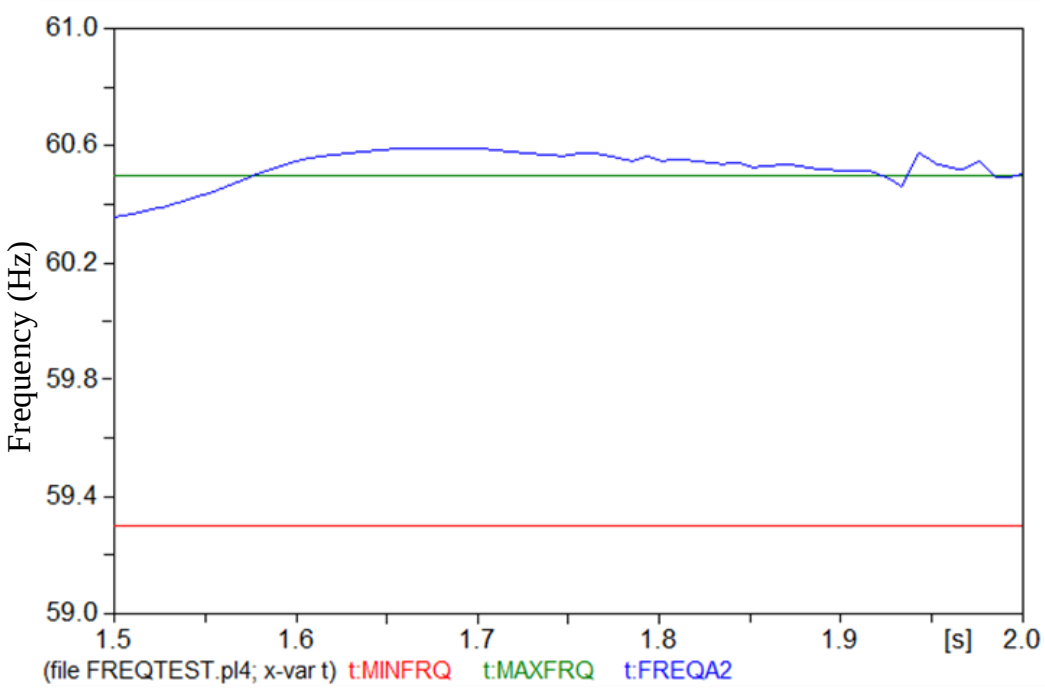

Figure 6.19: Frequency Level – Grid Side – FSC Test

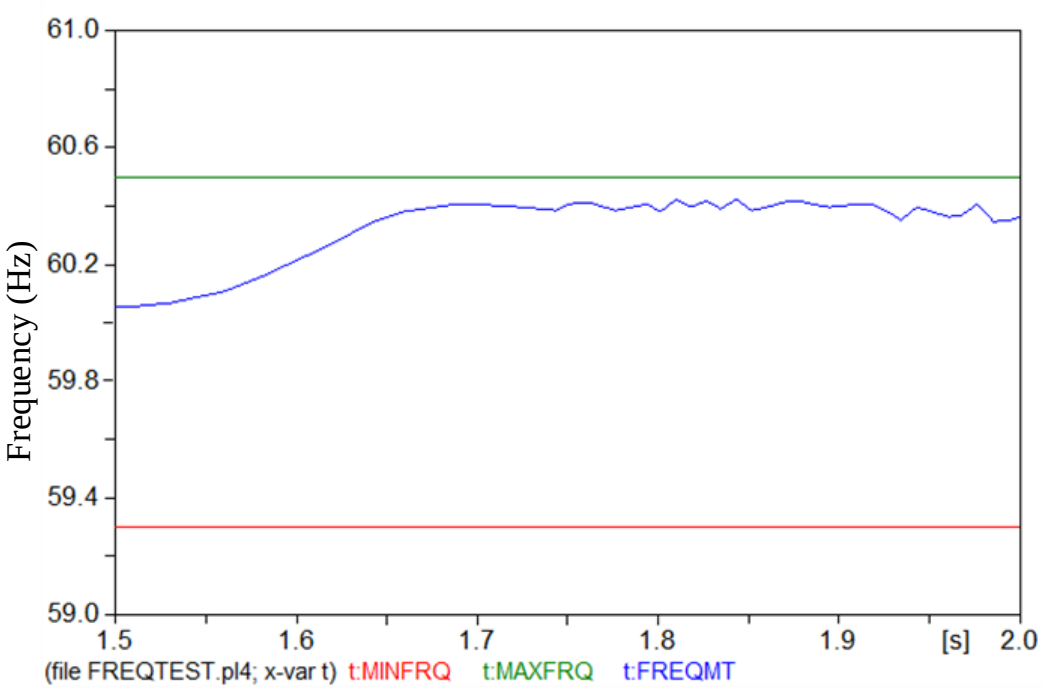

Figure 6.20: Frequency Level – Microgrid Side – FSC Test

6.3. Case B – Stand-Alone Simulation Results

In this test, results are obtained when the microgrid is disconnected from the main grid and it operated in an autonomous mode. Only the PCC 2 - microgrid side - measurements are presented while the other PCCs will be discussed in the observations subsection. Only the steady state reponse is tested under islanded microgrid operation. The microgrid is tested with and without a load shedding scheme to compare the results under two loading conditions.

6.3.1. Event B.1 - Normal Condition

Normal condition means that the system is simulated during a steady state condition, with no fault is applied, or any change in the system.

6.3.1.1. Unit A Terminal Voltage

The terminal voltage of unit A is acting properly and is not affected by the load condition. The voltage remains 11.26kV showing proper exciter performance. Figure 6.21 shows the terminal voltage response during islanded operation.

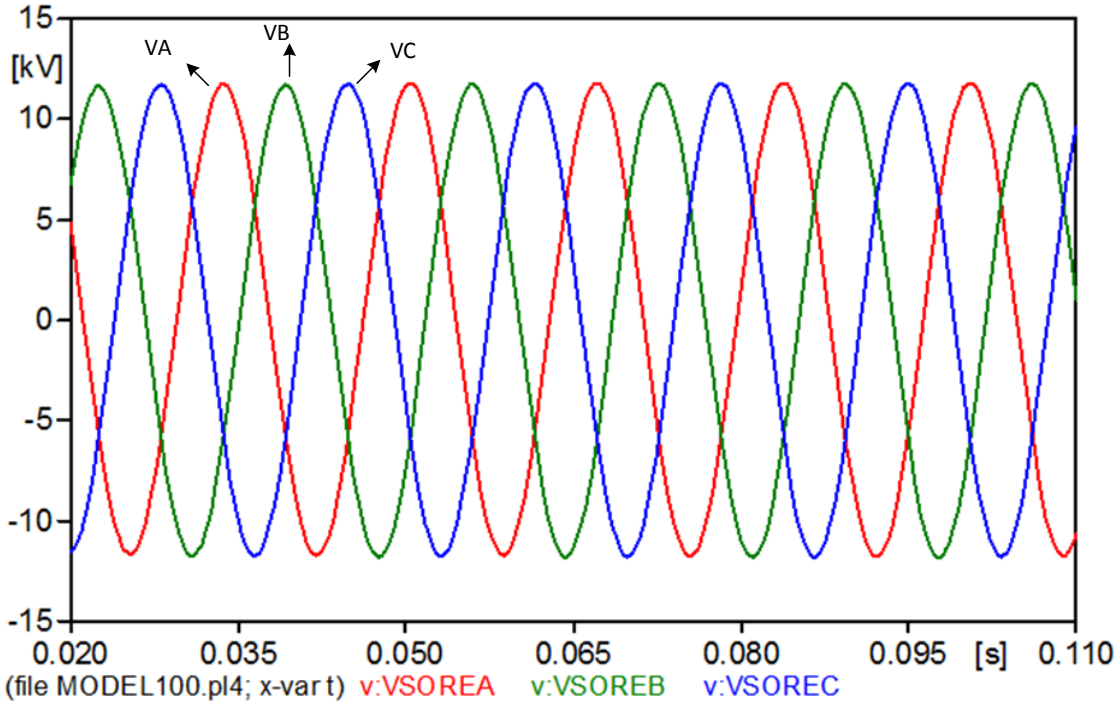

Figure 6.21: Unit A Terminal Voltage – Stand-Alone Normal Condition

6.3.1.2 PLL Frequency Tracking

Similar to the terminal voltage of unit A, the PLL is acting properly. Thus, the frequency is perfectly tracked as shown in Figure 6.22.

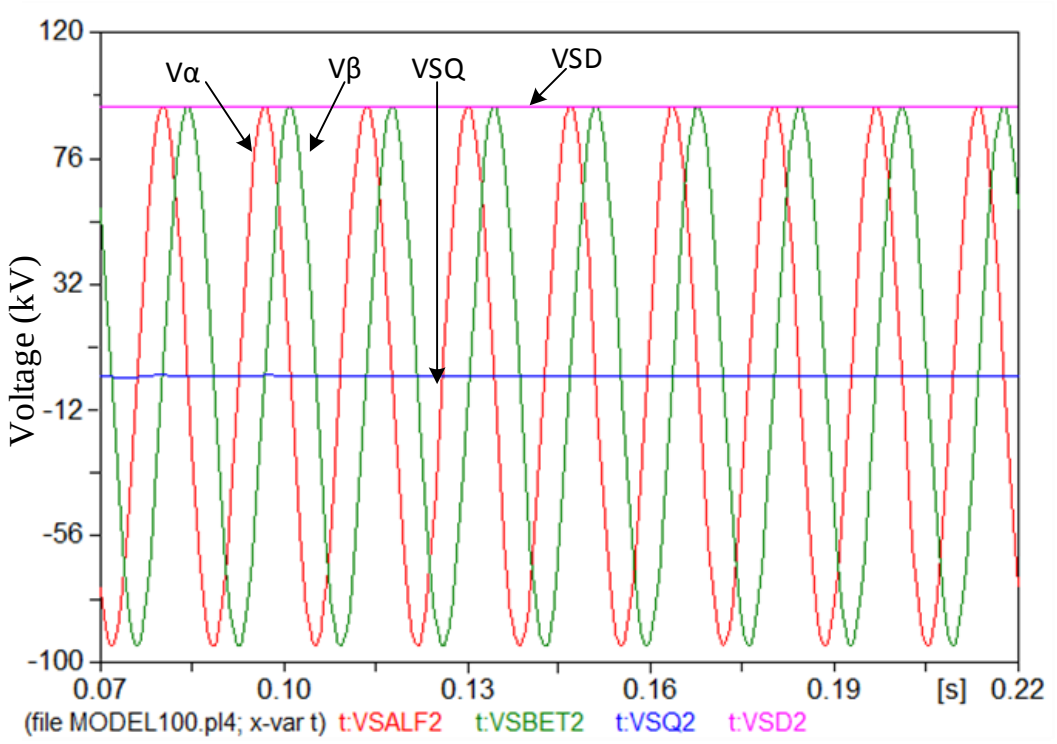

Figure 6.22: Frequency Tracking – Stand-Alone Normal Condition

6.3.1.3 OUV Scheme

The voltage level at the microgrid side of PCC2 dropped as a result of the switching to an islanded microgrid as shown in Figure 6.23. The voltage level is corrected after activating a load shedding scheme, with the voltage shown in Figure 6.24. The load shedding scheme is accomplished by dropping approximately 107 MW and 41MVAR of loads. Table 5.1 shows the total load of the microgrid during grid connected operation and Table 6.2 shows the total load of the microgrid during islanded mode.

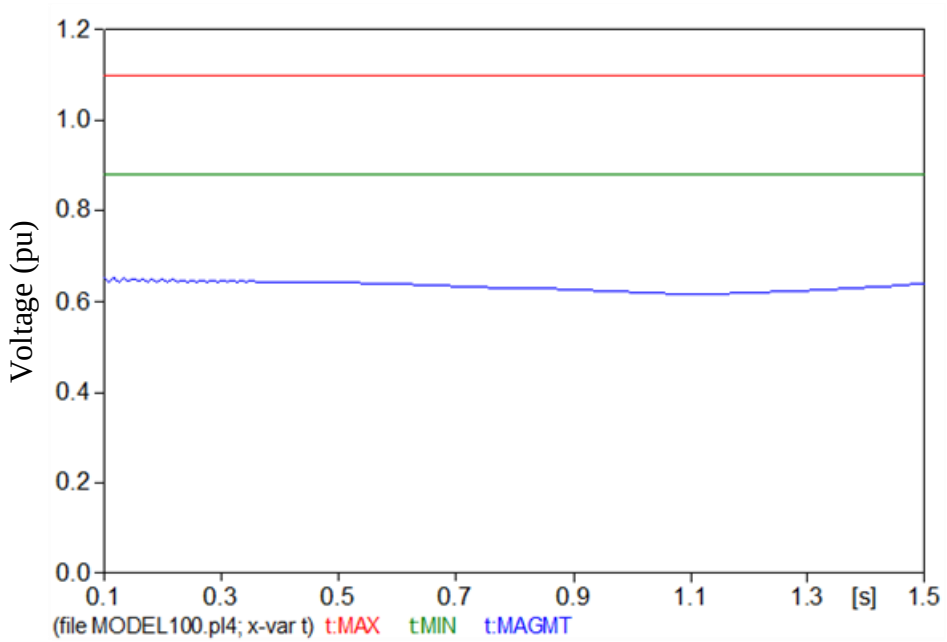

Figure 6.23: Voltage Level – Stand-Alone Normal Condition - without Load Shedding

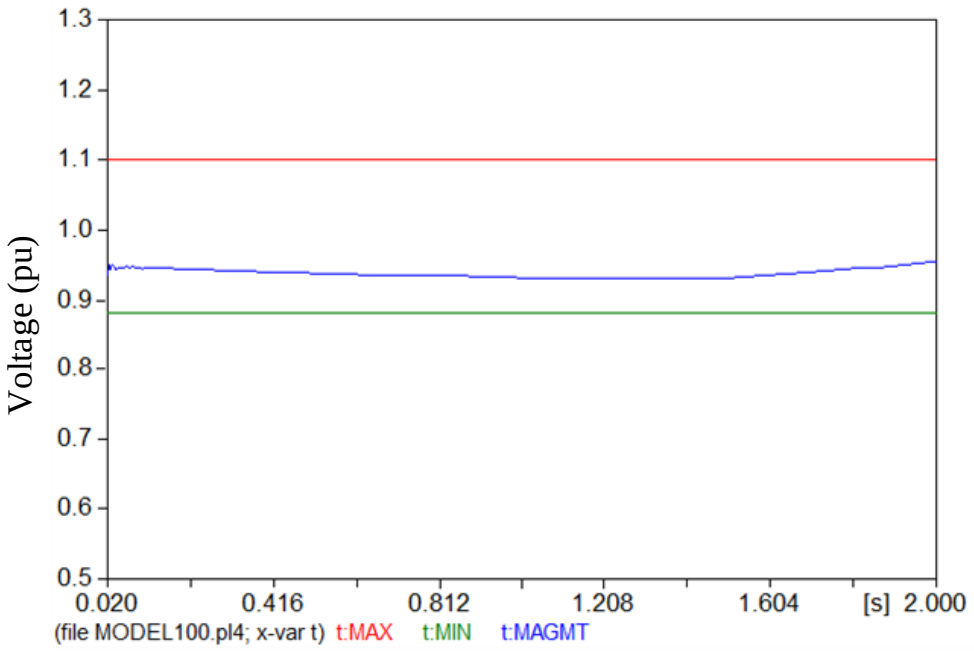

Figure 6.24: Voltage Level – Stand-Alone Normal Condition - with Load Shedding

6.3.1.4 OUF Scheme

Figures 6.25 and 6.26 show that the OUF scheme is not effected by the load shedding scheme during an isolated microgrid. The OUF will not pick up. In this case, the system is in microgrid operation before simulation starts.

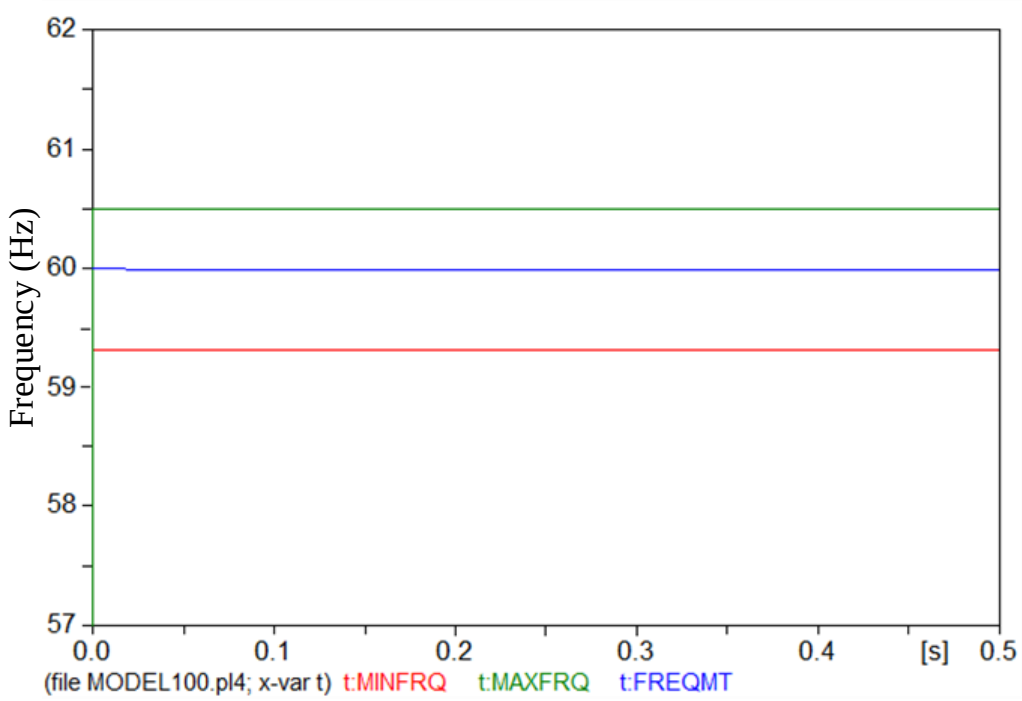

Figure 6.25: Frequency Level – Stand-Alone Normal Condition - without Load Shedding

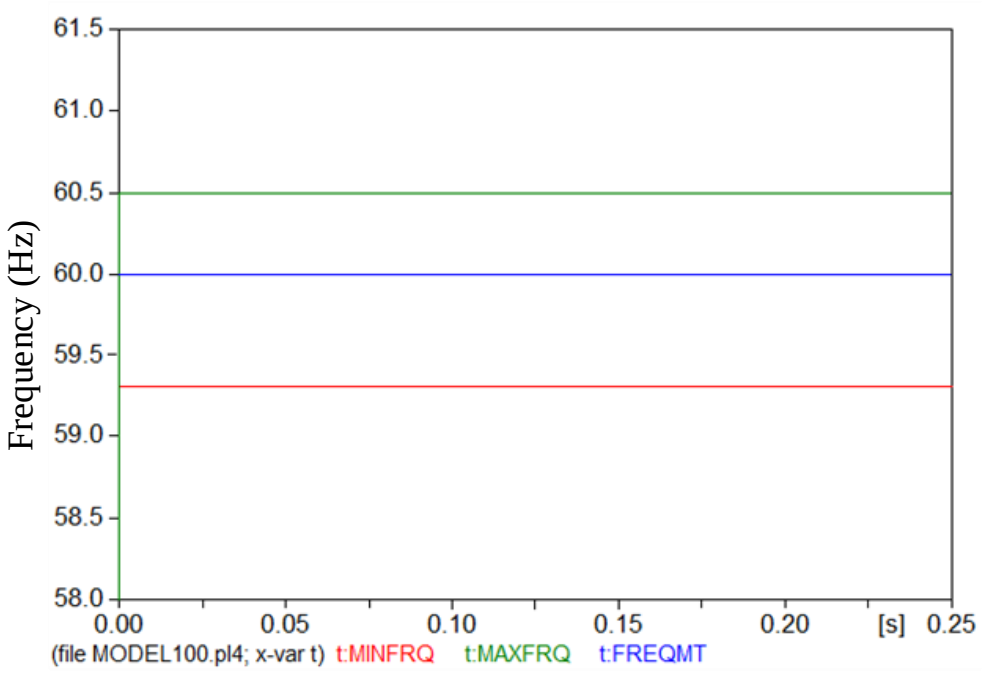

Figure 6.26: Frequency Level – Stand-Alone Normal Condition - with Load Shedding

6.4. Discussion of Results

In this section, the case A and B results are discussed in more details. Also, other interesting results not mentioned earlier are discussed.

6.4.1 Case A Discussion

This system is simulated during three system conditions while connected to the grid. The first condition is steady state operation. This is an important test as it makes sure that the system responds as expected and planned. The results show satisfactory outcomes where: the unit A terminal voltage magnitude is as expected, and the system frequency is tracked. Also, the OUV and OUF do not pick up which means that the microgrid remains in grid connected mode. The results matched the Powerworld case as well.

The second event is a SLG fault condition. Every power system is subject to fault conditions, therefore it is useful to test the system behavior under fault conditions and compare to expected behavior. SLG fault is chosen because this fault is the most common fault for overhead lines, among the fault types. The system studied uses overhead lines. The SLG fault case demonstrates that the OUV and OUF schemes are designed and worked properly because the schemes did not pick up under this case. Instead, during a loss of a major transmission line, which means a big system change, the schemes should pick up and detect the case.

A frequency swing condition is the third event that is tested in case A. The FSC test shows expected results for unit A machine where unit A terminal voltage should follow the system's frequency. If the frequency had changed from 60 Hz and settled in a new frequency and stayed there, the PLL would have properly tracked the new frequency. However, due to the the overlap between the 60 Hz and the low frequency component (0.5 Hz), the PLL fails to track the system frequency during FSC test. As a result, the OUV trips in this case because the voltage level at both sides of the PCC were under 0.88 pu for longer than 0.5 sec. The OUF did not detect an over frequency case at the grid side even though the frequency has exceeded the upper limit for only about 300 ms.

As shown in Figures 5.7 and 5.8, there is a counter associated with the schemes to ensure that they do not trip for a transient condition. To form an isolated microgrid, all the PCCs should experience abnormal condition, for a long period of time (500 ms – 1 sec), and in that case the circuit breakers on the PCC should give an open command. Table 6.1 provides a summary of case A results under varied system conditions.

Table 6.1: Summary of Case A Results

	Steady State	**SLG**	**FSC**
VT_Unit A	stable	effected	effected but tracked the system's voltage
PLL	tracked	tracked	not tracked
OUV_Scheme	not trip	not trip	counter hit the limit and tripped
OUF_Scheme	not trip	not trip	not trip

Usually the microgrid is operated in grid connected mode for the benefits discussed in Chapter 3. However, when the main grid experiences an abnormal condition, the microgrid has to detect the case and form an isolated microgrid. Therefore, the grid side voltage and frequency are monitored continuously to detect any variation in the voltage or frequency that causes the islanded operation condition. Figure 6.27 shows a flow diagram of the transition to a stand-alone microgrid.

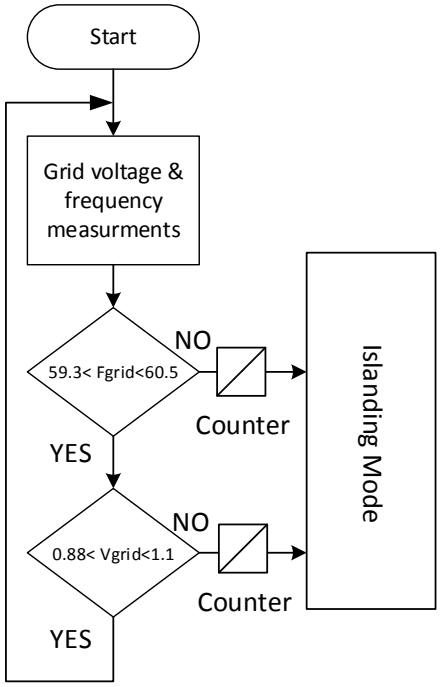

Figure 6.27: Microgrid Operation Procedure during Grid Connected Mode

6.4.2 Case. B Discussion

In this case the steady state behavior of the microgrid is tested under two load conditions. First, the microgrid is tested when it is switched to an isolated operation with the same load condition as occurred prior to the switching. In the first load condition, the total load of the microgrid is higher than the DGs' output capabilities. This is because the loads are designed to be fed from the bulk grid as well as the microgrid. Therefore, the OUV and OUF schemes pick up which means that the microgrid is not capable of supplying this level of load. This shows that a load shedding scheme needs to be developed.

The second load condition employs a load shedding scheme where load 3 and the capacitor bank in Figure 5.2 are disconnected because the voltage was too high. According to

the data from the project sponsor, the maximum load in the microgrid, high average load during the spring season, is 15.18 MW and 5.23 MVAR. This total load is divided to loads 1, 2, 3 and 4 based on system data. The loads are shown in Table 6.2.

Table 6.2: Load Shedding Ratings

	Real Power (MW)	**Reactive power (MVAR)**
Load 1	2.01771	0.95496
Load 2	11.336	3.48
Load 4 **(Load 3 is disconnected)**	1.82595	0.7938

The shedding technique achieves the desirable result such that the voltages are within the acceptable range, and the OUV elements are not picked up. Therefore, the microgrid successfully meets the IEEE 1547 requirements for stand-alone operation. Table 6.2 summaries Case B results.

Table 6.3: Summary of Case B Results

	Steady State Condition	
	No Load Shedding	**With Load Shedding**
VT_Unit A	not effected	not effected
PLL	tracked	tracked
OUV_Scheme	picked up	not picked up
OUF_Scheme	not picked up	not picked up

The OUV scheme picked up during the no load shedding case because the microgrid load was higher than the DGs power capability. Therefore, the microgrid load was dropped by 107 MW and 41MVAR.

6.4.3 Other Observations

Some other interesting outcomes can be observed in the simulation results.

- At the same time as the response of PCC2 is monitored for the varied system conditions, the other three PCCs were simulated and monitored. They show results consistent with those at PCC2, thus only PCC2 was chosen to represent the behavior of the all PCCs.
- The results for the SLG fault condition on microgrid side during grid connected and isolated modes are as comparable to the case when SLG fault is applied to the main grid side. However, in Figure 6.28, SLG fault is applied to the microgrid close to PCC2, which means the location of the SLG fault changed. The OUV scheme picks up under this case. Therefore, when the fault occurs on the transmission line of the microgrid, PCC2 side, the voltage will fall outside the OUV threshold, but not for a sufficient time to trigger the element and incorrectly form a microgrid. On the other hand, Figure 6.29 shows that the OUV does not pick up for fault close to the DG side.

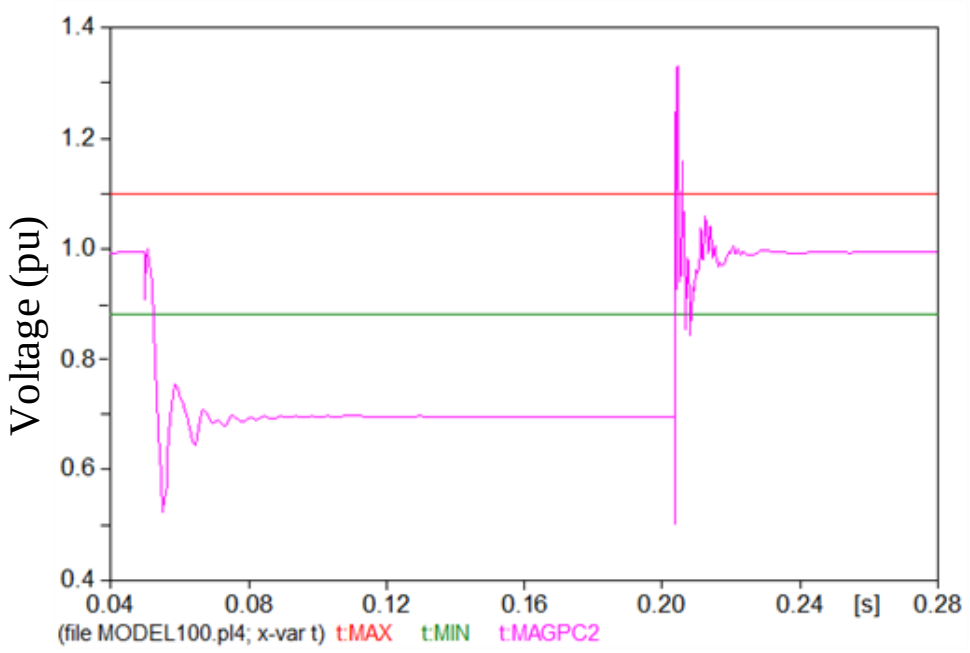

Figure 6.28: Voltage Level - SLG Fault on the Microgrid– close to PCC2

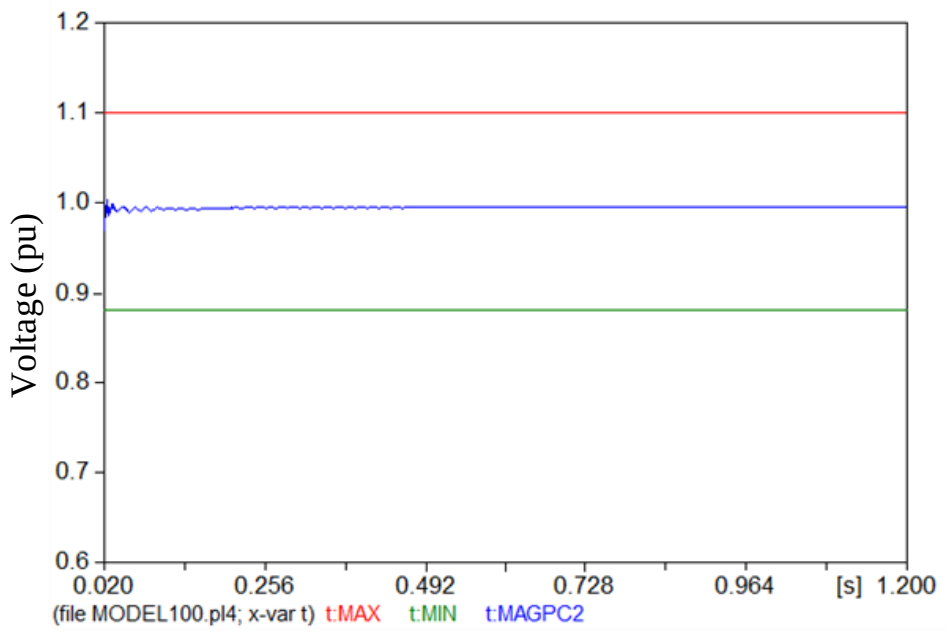

Figure 6.29: Voltage Level - SLG Fault on Microgrid– close to DG A

- The isolated microgrid can be reconnected to the main grid when the abnormal condition on the main grid is cleared. The voltages, frequencies, and phase angles across the connected CB at the PCC need to be matched to enable the synchronization between the two systems. Figure 6.30 illustrates the microgrid reconnection procedure.

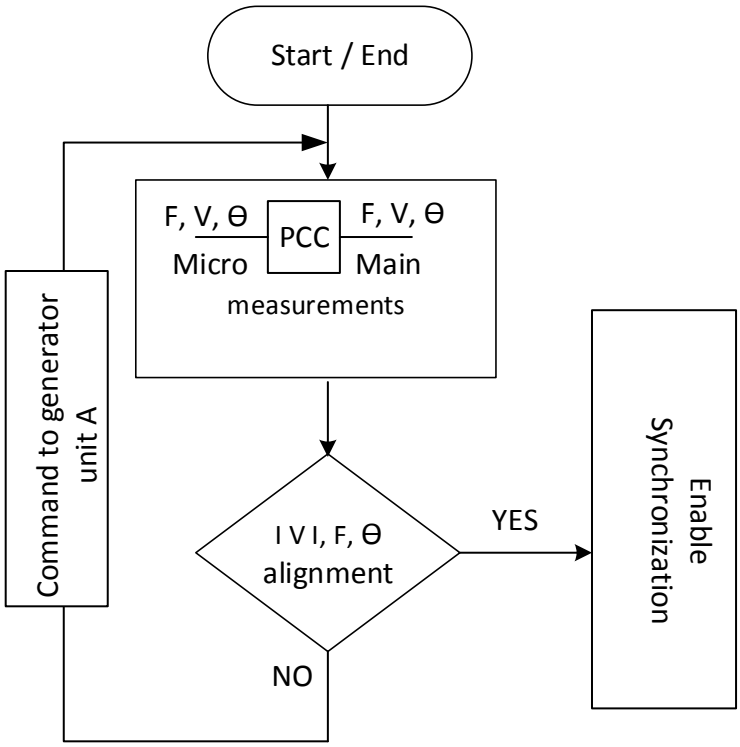

Figure 6.30: Microgrid Reconnection Procedure

Chapter 7: Summary, Conclusions and Future Work

7.1 Summary

This thesis addressed several topics related to the concept of microgrid operation and control. Two important topics related to microgrids were explained: synchronization and islanding detection schemes. After that, a detailed microgrid model for a medium sized city in the Pacific Northwest was built, based on two hydro generators feeding four critical loads. These four loads are connected to four substations, with each substation also connected to the main grid through a PCC. Four Thevenin sources are designed to represent the connection to the main grid. Within the microgrid, a detailed model of one of the generators is built including excitation and governer schemes. Also, different control circuits were developed for synchronization tracking, and for monitoring the voltages/frequencies for detecting conditions warranting islanding formation. Multiple studies have been conducted when the microgrid is in grid connected mode during normal, SLG faults, and frequency swing conditions. Then, the microgrid operation has been tested during normal condition in stand-alone mode. Finally, the simulation results were evaluated and discussed.

7.2 Conclusions

The microgrid built in this thesis demonstrates the effects of multiple system conditions on microgrid control schemes using an actual metropolitan downtown network as a test study. Microgrid operation response during grid connected and isolated modes have different behavior. Therefore, this research aims presented a possible plan for achieving a successful microgrid integration in the field.

The simulation results reveal that the control schemes that are built in this thesis worked as expected. The results of unit A terminal voltage during the different test conditions proved that unit A machine is designed and built correctly. Also, the over/under voltage and over/under frequency islanding detection schemes worked properly. The PLL control circuit successfully tracked the system's frequency, except during the FSC test where the PLL could not track the frequency due to the rate of the swing.

The simulation results also showed that the microgrid and main grid will both be effected during abnormal conditions. Thus, the interconnection point between the bulk power system and microgrid should be equipped with protection devices that monitor the voltages, frequencies and phase angles to ensure better detection for a system conditions. The PCCs should be coupled with high speed communication schemes or at least traditional SCADA to allow communication between the PCC and DGs in the microgrid.

It is important for a system to distinguish between a temporary power quality disturbance and an interruption condition that requires forming a microgrid. During temporary disturbances, the over/under voltage and over/under frequency monitoring schemes will react, but won’t pick unless the condition last for a long time, ensuring accurate detection of conditions requiring islanding.

7.3 Future Work

This thesis has started development microgrid platform model that can be used for multiple studies in the future. Some suggested improvements to the model and possible studies are described below.

- Study the possibility of adding additional generator sources. The proposed location has potential for the addition of renewable energy sources such as PV and wind turbines. Therefore, to further study the microgrid potential, a study of the microgrid response with voltage-source converter interfaced generators is suggested. This also suggests another interesting study: since most of the power electronic interfaced DG are inertialess sources, investigating their impacts on the microgrid stability and controllability would be important for the site at hand.
- A detailed model for unit B would provide a much more accurate model of the impact of the DGs in the microgrid in isolated status. It will be important to develop and test the generators' exciters and governors and conduct transient studies to build droop control schemes within the microgrid. Since unit A was used as a master generator, applying different control schemes (such as droop control scheme) and comparing the results with master-slave technique will be useful. These additions will make the model a more accurate representation of a real system.
- Protection studies can be performed on this model. Different protection schemes can be built for both the microgrid and main grid sides to ensure a proper response during abnormal conditions. A reliable and secure scheme to trigger settings changes for the protection devices between the grid connected and islanded operation is an interesting topic. In this case methods to change the relay settings upon transition to microgrid need to be investigated. One of the challenges is the setting of overcurrent elements. The time coordination

between overcurrent relays need to be considered when switching from grid connected to islanded mode. Overcurrent relays may be replaced with differential elements; however, differential elements are more costly compared to overcurrent elements.

- Study of detailed load shedding schemes and control, as well as real and reactive power PQ management is recommended. These studies are needed to ensure a successful transition to islanding operation, where a set of priority loads will be preserved according to a number of DGs in the microgrid.
- Testing the microgrid while in stand-alone mode during the dynamic response to load changes was not conducted in this study. Thus, continuing the procedure and comparing the results with the grid connected results would be interesting. Also, testing the microgrid operation during different fault types other than SLG with including the effect of the fault resistance, and observing the differences between them will yield useful information.

References

[1] M. Allehyani, H. Samkari, B.K. Johnson, “Modeling and Simulation of the Impacts of STATCOM Control Schemes on Distance Elements,” accepted for presentation at the 2016 North American Power Symposium.

[2] J. B. Roberts, A Guzman, and E. O. Schweitzer, III, “Z = V/I does not make a distance relay,” *20th Annual Western Protective Relay Conference*, Spokane, WA, October 19-21, 1993. Available: http://www.selinc.com 6/20/2016

[3] E.O. Schweitzer and H.J. Altuve, *Modern Solutions for Protection, Control, and Monitoring of Electric Power Systems*, Pullman: Schweitzer Engineering Laboratories, Inc., 2010

[4] R.K. Varma, "Introduction to FACTS Controllers," *Power Systems Conference and Exposition, 2009. PSCE '09. IEEE/PES*, Seattle, WA, 2009, pp. 1-6

[5] F.A. Albasri, T.S. Sidhu, R.K. Varma, "Performance Comparison of Distance Protection Schemes for Shunt-FACTS Compensated Transmission Lines,” *IEEE Transactions on Power Delivery* , vol. 22, no. 4, pp. 2116-2125, Oct. 2007

[6] D. Hemasundar, M. Thakre, V.S. Kale, "Impact of STATCOM on distance relay - Modeling and simulation using PSCAD/EMTDC," *Electrical, Electronics and Computer Science (SCEECS), 2014 IEEE Students' Conference on*, Bhopal, 2014, pp. 1-6

[7] F.A. Albasri, T.S. Sidhu, R.K. Varma, "Impact of Shunt-FACTS on Distance Protection of Transmission Lines," *2006 Power Systems Conference: Advanced*

Metering, Protection, Control, Communication, and Distributed Resources, Clemson, SC, 2006, pp. 249-256

[8] H. Samkari, M. Allehyani, B.K. Johnson, "Modeling and Simulation the Impacts of STATCOMs on Distance Protection," *North American Power Symposium (NAPS), 2015*, Charlotte, NC, 2015, pp. 1-5

[9] A. Yazdani and R. Iravani, *Voltage-sourced Converters in Power Systems*, New Jersey: John Wiley & Sons, Inc., 2010

[10] M.V. Sham, K.S. Chethan, K.P. Vittal, "Development of adaptive distance relay for STATCOM connected transmission line," *Innovative Smart Grid Technologies - India (ISGT India), 2011 IEEE PES*, Kollam, Kerala, 2011, pp. 248-253

[11] IEEE Power Systems Relaying Committee, *Use of Synchrophasor Measurements in Protective Relaying Applications*. Report of Working Group C-14 of the System Protection Subcommittee. April 2013.

[12] Liu Qing; Wang Zeng-ping; Zhang Yuan, "Study on a Novel Method of Distance Protection in Transmission Line with STATCOM," *2010 Asia-Pacific Power and Energy Engineering Conference*, Chengdu, 2010, pp. 1-5

[13] E. O. Schweitzer, III, "New Developments in Distance Relay Polarization and Fault Type Selection," *16th Annual Western Protective Relay Conference, Spokane*, WA, October 24-26, 1989. Available: http://www.selinc.com 6/20/2016

[14] J.L. Blackburn, T.J. Domin, *Protective Relaying Principles and Application, 4th Ed*., NewYork:Taylor & Francis Group, LLC, 2014

[15] G. Andersson et al., "Causes of the 2003 major grid blackouts in North America and Europe, and recommended means to improve system dynamic performance," *IEEE Transactions on Power Systems*, vol. 20, no. 4, pp. 1922-1928, Nov. 2005.

[16] X. Zhou, T. Guo and Y. Ma, "An overview on microgrid technology," *2015 IEEE International Conference on Mechatronics and Automation (ICMA)*, Beijing, 2015, pp. 76-81.

[17] A. V. Jayawardena, L. G. Meegahapola, S. Perera and D. A. Robinson, "Dynamic characteristics of a hybrid microgrid with inverter and non- inverter interfaced renewable energy sources: A case study," *Power System Technology (POWERCON), 2012 IEEE International Conference on*, Auckland, 2012, pp. 1-6.

[18] *IEEE Standard for Interconnecting Distributed Resources with Electric Power Systems*, IEEE Standard 1547, 2003

[19] B. Kroposki, R. Lasseter, T. Ise, S. Morozumi, S. Papathanassiou and N. Hatziargyriou, "Making microgrids work," *IEEE Power and Energy Magazine*, vol. 6, no. 3, pp. 40-53, May-June 2008

[20] Wei Huanga, Miao Lua, Li Zhangb, "Survey on Microgrid Control Strategies," *Proceedings of International Conference on Smart Grid and Clean Energy Technologies (ICSGCE)* 27–30 September 2011. Available: http://www.sciencedirect.com 6/16/2016

[21] F. Katiraei, C. Abbey, S. Tang and M. Gauthier, "Planned islanding on rural feeders — utility perspective," *Power and Energy Society General Meeting - Conversion and*

Delivery of Electrical Energy in the 21st Century, 2008 IEEE, Pittsburgh, PA, 2008, pp. 1-6.

[22] H. Xu *et al*., "Synchronization strategy of microgrid from islanded to grid-connected mode seamless transfer," *TENCON 2013 - 2013 IEEE Region 10 Conference (31194)*, Xi'an, 2013, pp. 1-4.

[23] D. L. Ransom, "Get in Step With Synchronization," *IEEE Transactions on Industry Applications*, vol. 50, no. 6, pp. 4210-4215, Nov.-Dec. 2014.

[24] *Introduction to Synchronizing Automatic Synchronizing Considerations and Applications* available on http://www.ussg.com.sa/pdf2.pdf 6/2/2016

[25] A. Timbus, M. Liserre, R. Teodorescu and F. Blaabjerg, "Synchronization methods for three phase distributed power generation systems - An overview and evaluation," *2005 IEEE 36th Power Electronics Specialists Conference*, Recife, 2005, pp. 2474-2481.

[26] R. Teodorescu, M. Liserre, P. Rodriguez, "Islanding Detection," *Grid Converters for Photovoltaic and Wind Power Systems* , Wiley-IEEE Press, 2011, pp.93-122.

[27] O. Samuelsson and N. Strath, "Islanding detection and connection requirements," *Power Engineering Society General Meeting, 2007. IEEE*, Tampa, FL, 2007, pp. 1-6.

[28] M. Ropp, and W. Bower, "Evaluation of islanding detection methods for photovoltaic utility interactive power systems," *International Energy Agency Implementing agreement on Photovoltaic Power Systems*, Tech. Rep. IEA PVPS T5-09, March 2002.

[29] H. Zeineldin, Weidong Xiao and Ali Kasem Alaboudy, "Performance of frequency relays with multiple synchronous based DG units," *Industrial Electronics (ISIE), 2012 IEEE International Symposium on*, Hangzhou, 2012, pp. 1616-1620.

[30] J. C. M. Vieira, W. Freitas, Z. Huang, W. Xu and A. Morelato, "Formulas for predicting the dynamic performance of ROCOF relays for embedded generation applications," *IEE Proceedings - Generation, Transmission and Distribution*, vol. 153, no. 4, pp. 399-406, 13 July 2006.

[31] *IEEE Standard Conformance Test Procedures for Equipment Interconnecting Distributed Resources with Electric Power Systems*, IEEE Standard 1547.1, 2005.

[32] *IEEE Application Guide for IEEE Std 1547(TM), IEEE Standard for Interconnecting* Distributed Resources with Electric Power Systems, IEEE Standard 1547.2, 2009.

[33] *IEEE Guide for Monitoring, Information Exchange, and Control of Distributed Resources Interconnected with Electric Power Systems*, IEEE Standard 1547.3, 2007.

[34] *IEEE Guide for Design, Operation, and Integration of Distributed Resource Island Systems with Electric Power Systems*, IEEE Standard 1547.4, 2011.

[35] *IEEE Recommended Practice for Interconnecting Distributed Resources with Electric Power Systems Distribution Secondary Networks*, IEEE Standard 1547.6, 2011.

[36] *IEEE Approved Draft Guide to Conducting Distribution Impact Studies for Distributed Resource Interconnection*, IEEE Standard P1547.7/D11, 2014.

[37] *IEEE Recommended Practice for Excitation System Models for Power System Stability Studies*, IEEE Standard 421.5, 2005.

[38] NEPLAN http://www.neplan.ch/ 6/6/2016

[39] *IEEE Recommended Practice for Preparation of Equipment Specifications for Speed-Governing of Hydraulic Turbines Intended to Drive Electric Generators*, ANSI/IEEE Standard 125, 1988.

[40] R. H. Lasseter, et at., *Electromagnetic Transients Program (EMTP) Workbook IV*, EPRI EL-4651, volume 4, 1989. Available on: http://www.epri.com 07/12/2016

Appendix A – Power System Model Parameters and Over/Under reach Explanation

This appendix is related to Chapter 2, and provides some information and explanation about the tested model. Figure A.1 shows the system model in ATP.

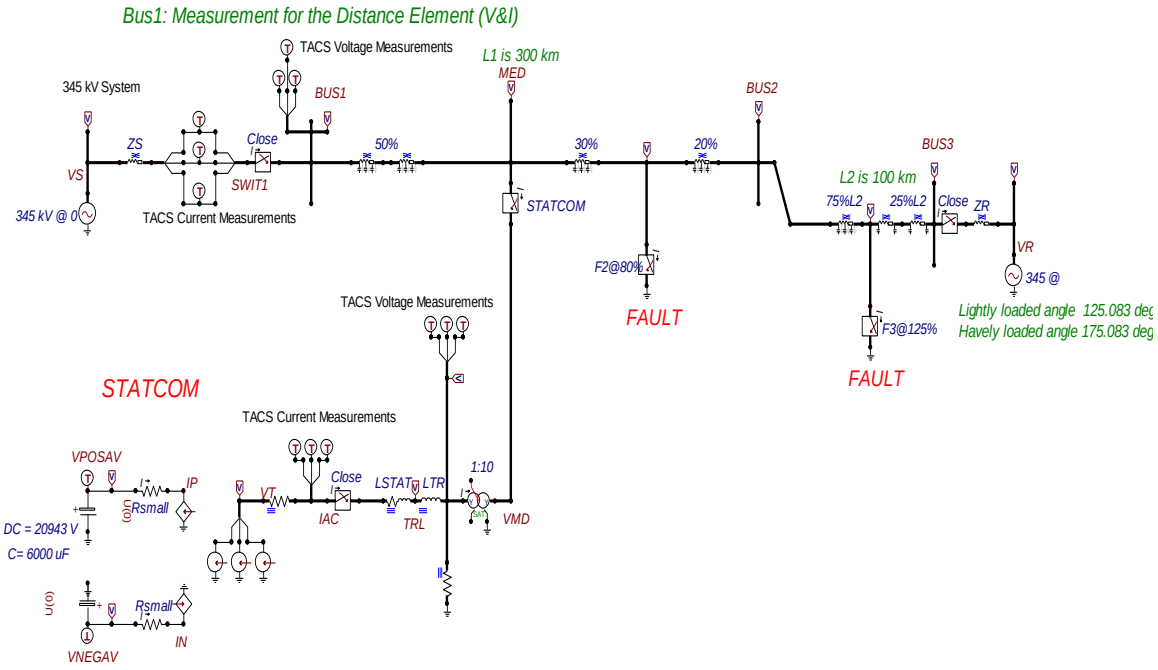

Figure A.1: The ATP Model of the Power System

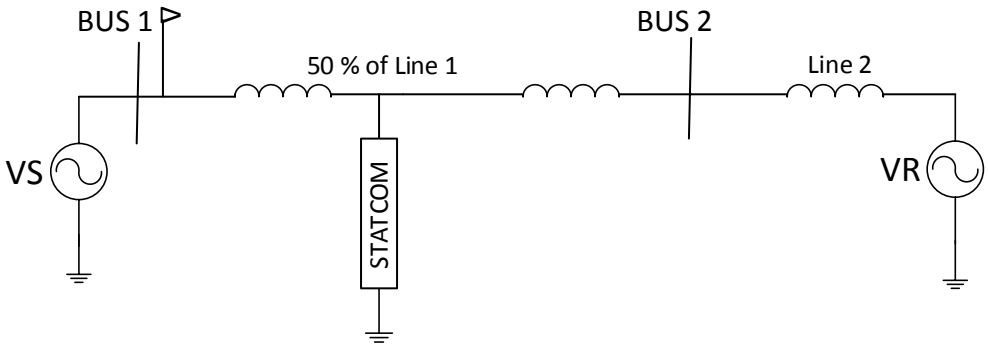

Figure A.2: Power System Model Diagram

Power Model Parameters

Z_{s1} = (0.238 + 5.72i) ohm Z_{r1} = (0.238 + 6.19i) ohm

Z_{s0} = (2.738 + 10i) ohm Z_{r0} = (0.833 + 5.12i) ohm

$Z_{line1\_1} = Z_{line2\_1}$ = (0.028 + 0.507i) ohm / km Line1_length = 300 km

$Z_{line1\_0} = Z_{line2\_0}$ = (0.275 + 1.404i) ohm / km Line2_length = 100 km

Z_{stat_lead} = (0.00588 + 0.26012i) ohm Z_{xfmr} = 0.15 pu

C_line1_1 = 1.422 μF C_line1_0 = 1.006 μF

C_line2_1 = 0.948 μF C_line2_0 = 0.671 μF

S_{base} = 100 MVA Cap = 6000 μF

K_0 = 0.597 – 0.13i

Relay Model Parameters

In the relay model, the current and voltage transformers are assumed ideal; where the ratio of the measurement devices are CTR = 1, PTR = 1

Set up the M-equation reach setting for zone 2 (120% of Line 1 impedance):

$Z_{1MAG} = 1.2\ |Zline1|$ (A.1)

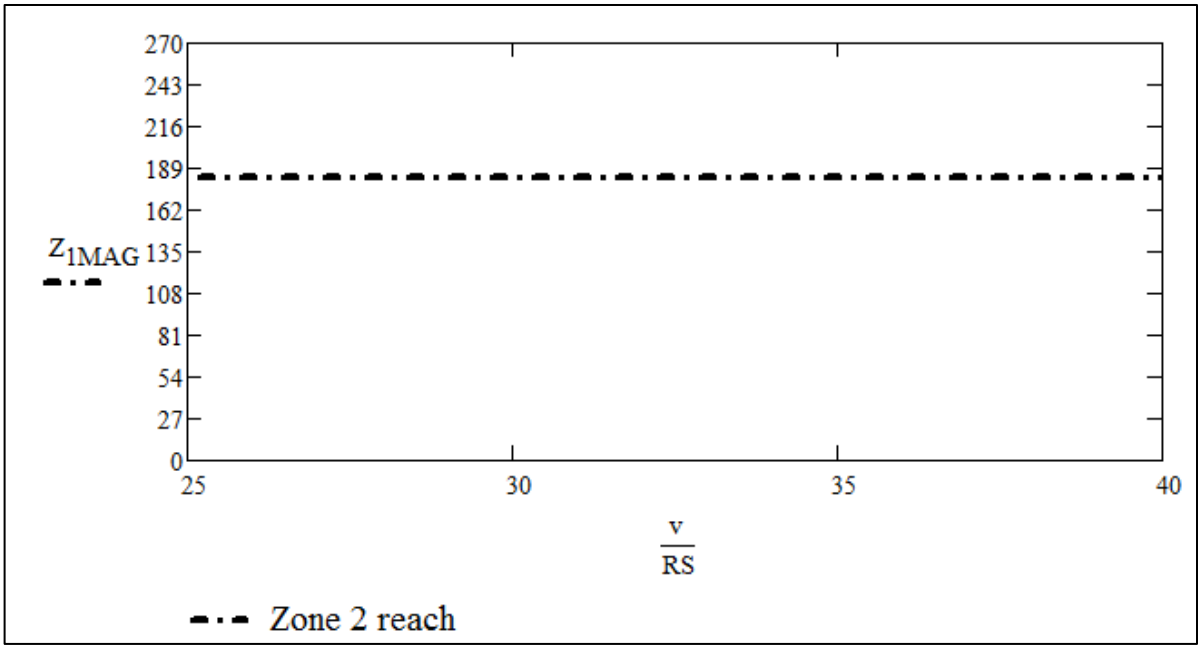

Figure A.3: Zone 2 Reach Setting for the Distance Element

Overreach Versus Underreach:

When the STATCOM is present in the fault loop, the voltage and current signals at the relay point will be affected in both steady and transient state. This impact will affect the performance of distance relay.

$$Z_{relay} = \frac{V_{measured}}{I_{measured}} \quad \text{(A.2)}$$

Overreach Case

Overreach occurs when the distance element will trip for faults out of the setting reach. Here, zone 2 is set to reach 120% of line 1. The fault applied at 125% and the relay detect a fault condition.

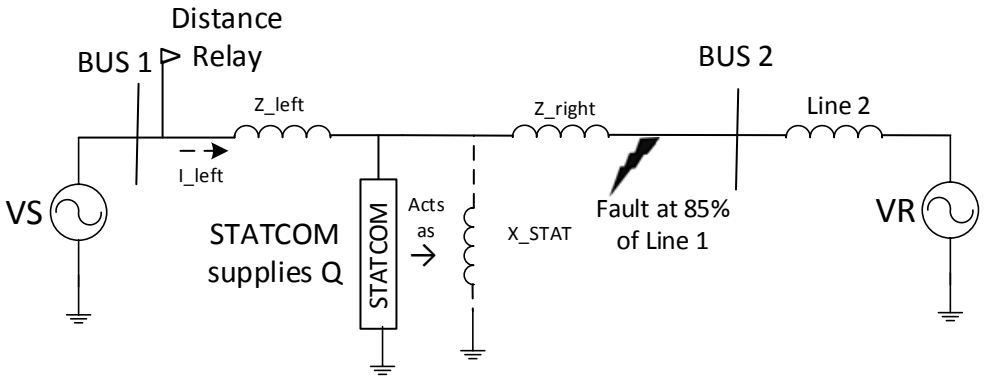

Figure A.4: Circuit Diagram during Overreach Condition

The distance element in equation (A.1) measures a lower impedance when STATCOM is used to absorb reactive power. Therefore, the distance element always overreaches when STATCOM is inside the fault loop and absorb reactive power.

Underreach Case

When underreach occures the distance element will not trip for faults inside the setting reach. Here, zone 1 is set to reach 80% of line 1. If a fault is applied at 75% and the relay will fail to detect a fault condition if it underreaches by more than 5%.

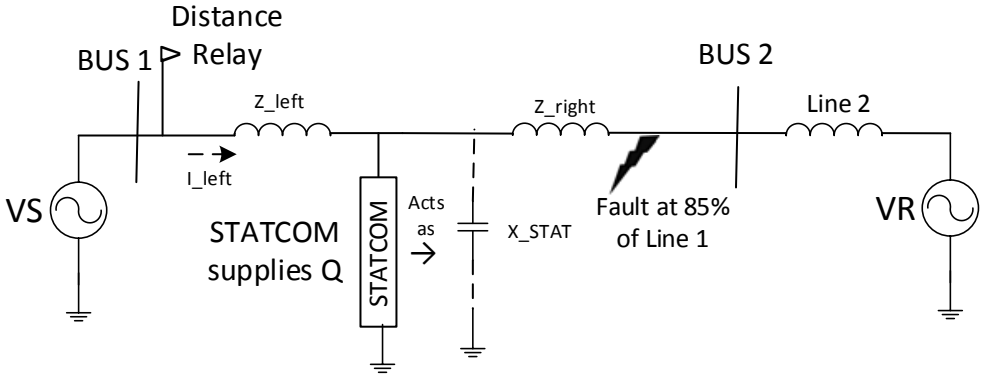

Figure A.5: Circuit Diagram during Underreach Condition

Effectively the distance element in equation (A.1) measures a bigger impedance when STATCOM is used to supply reactive power. Therefore, the distance element always underreaches when STATCOM is inside the fault loop and supply reactive power.

Mathematical Explanation

The overreach/underreach condition can be demonstrated as Figure A.6 based on current equations as below. There will be a voltage drop across the STATCOM impedance; as a result of the STATCOM current. This current – as magnitude and direction – would create an apparent impedance between the STATCOM and the fault location. The following equations demonstrat the effect of the STATCOM current on the distance relay.

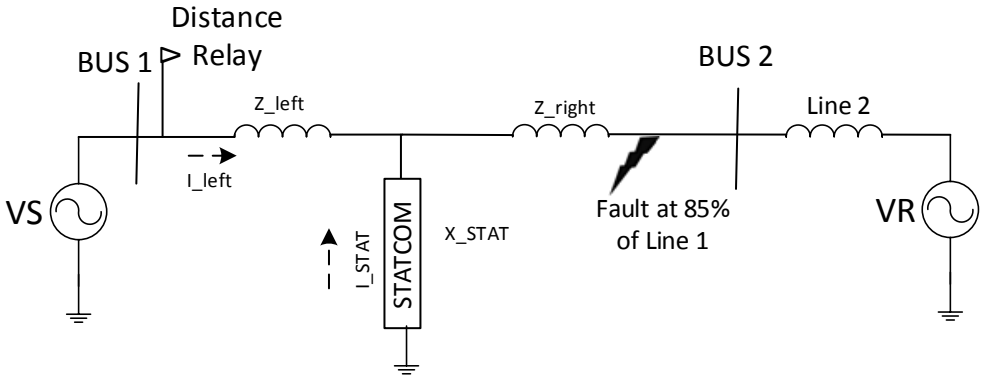

Figure A.6: Underreach/Overreach Explanation Diagram

$$V_{BUS1} = I\_left * Z\_left + (I\_left + I\_STAT) * Z\_right \quad (A.3)$$

$$Z_{relay} = \frac{VBUS1}{I\_left} = Z\_left + Z\_right \left(1+\frac{I\_STAT}{I\_left}\right) \quad (A.4)$$

Therefore, if the current ratio between I_STAT and I_left is positive (I_STAT = inductive, STATCOM supplies reactive power), the distance element will measure a bigger impedance and will underreach. However, if the ratio is negative (I_STAT = capacitive, STATCOM

absorbs reactive power), the distance element will measure a decreased impedance and will overreach.

Appendix B – Microgrid Model Parameters and Circuits

This appendix provides additional information to support the second topic, Control studies for a microgrid in a medium sized city in the Pacific Northwest.

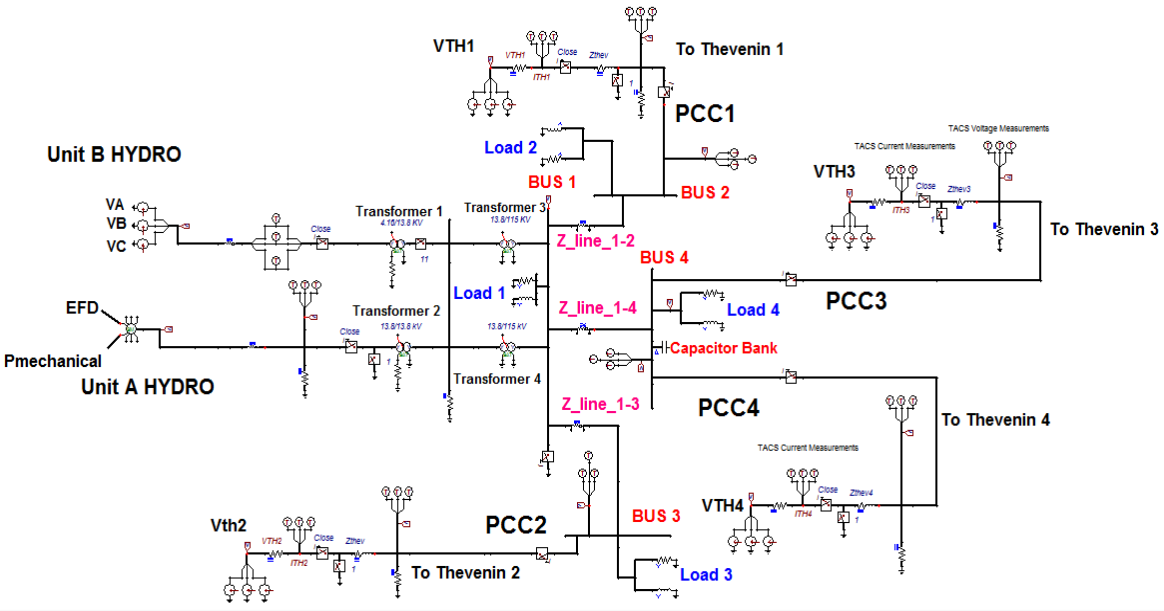

Figure B.1: The Power Model of the ATP Circuit for the Microgrid

Power Model Parameters

Transmission Line Parameters:

Table B.1: Transmission Line Parameters of the Power System

	Z_Line_1-2	**Z_Line_1-3**	**Z_Line_1-4**
R_+ve seq,-ve seq	0.02248 Ω	0.02116 Ω	0.2499525 Ω
R_zero seq	0.056206 Ω	0.0529 Ω	0.6248813 Ω
L_+ve seq,-ve seq	0.4981417 mH	0.4420131 mH	2.8029241 mH
L_zero seq	1.2453543 mH	1.1050327 mH	7.0073103 mH
C_+ve seq,-ve seq	0.1227509 µF	0.1550432 µF	0.1867338 µF
C_zero seq	0.1227509 µF	0.1550432 µF	0.1867338 µF

Transformer Parameters:

Table B.2: Transformers Parameters of the Power System

	R (pu)	**X (pu)**
Transformer 1	0.032638	0.564108
Transformer 2	0.01655	0.25945
Transformer 3	0.021628	0.63276
Transformer 4	0.022237	0.643655

Control Circuits:

Unit A Exciter Implementation

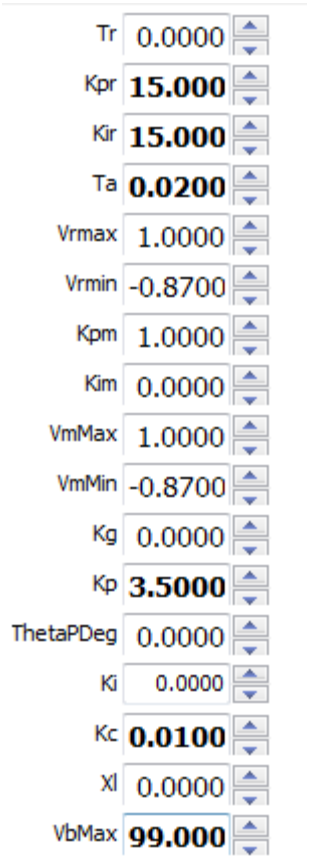

Figure B.2: Unit A Exciter Parameter

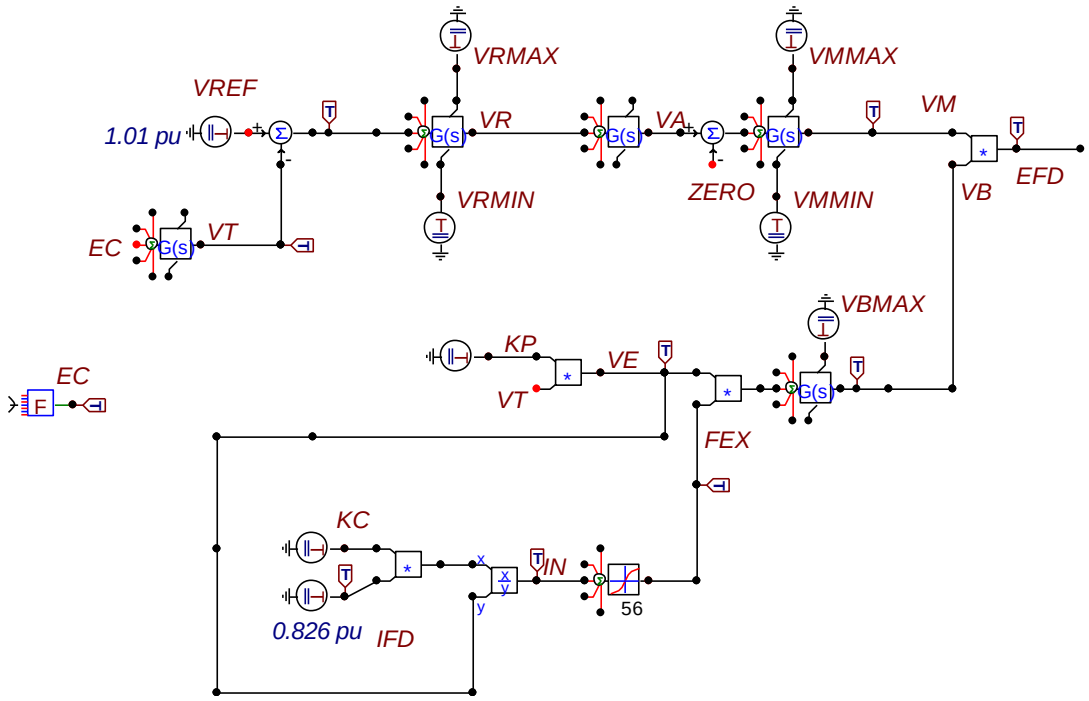

Figure B.3: Control Block Diagram for Unit A Exciter

EC, for the voltage compensator, in Figure B.3 is calculated as

$$EC = \frac{\sqrt{(V_{unitA-d\ axis})^2+(V_{unitA-q\ axis})^2}}{V_{uniA\ Base}} \quad \text{(B.1)}$$

Unit A Governor Implementation

Rperm	0.0400	At	1.2000	Gv0	0.0000	Pgv4	0.0000	Bgv5	0.0000
Rtemp	0.3000	Dturb	0.5000	Pgv0	0.0000	Gv5	0.0000	Bmax	0.0000
Tr	5.0000	Qnl	0.0500	Gv1	0.0000	Pgv5	0.0000	Tblade	100.0000
Tf	0.0500	Ttur	0.5000	Pgv1	0.0000	Hdam	1.0000	Trate	0.0000
Tg	0.5000	Tn	0.0000	Gv2	0.0000	Bgv0	0.0000		
Velm	0.2000	Tnp	0.0000	Pgv2	0.0000	Bgv1	0.0000		
Gmax	1.0000	db1	0.0000	Gv3	0.0000	Bgv2	0.0000		
Gmin	0.0000	Eps	0.0000	Pgv3	0.0000	Bgv3	0.0000		
Tw	1.0000	db2	0.0000	Gv4	0.0000	Bgv4	0.0000		

Figure B.4: Unit A Governor Parameter

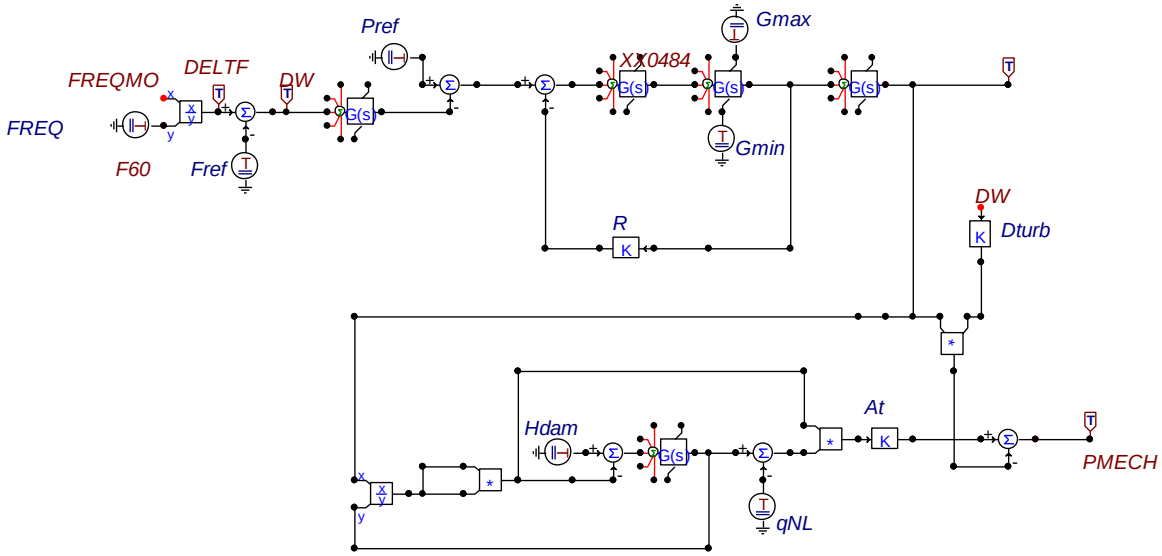

Figure B.5: Control Block Diagram for Unit A Governor

Unit A Generator Parameters

H	**1.7500**	Tdop	**5.0000**
D	0.0000	Tqop	**0.0000**
Ra	0.0000	Tdopp	**0.0300**
Xd	**0.9000**	Tqopp	0.0500
Xq	**0.6000**	S1	**0.2000**
Xdp	**0.2930**	S12	**0.5500**
Xqp	**0.6000**	RComp	0.0000
Xdpp	**0.2680**	XComp	0.0000
Xqpp	**0.2680**	Accel	**0.5000**
Xl	**0.2300**	Kis	**0.0600**

Figure B.6: Unit A Generator Parameters

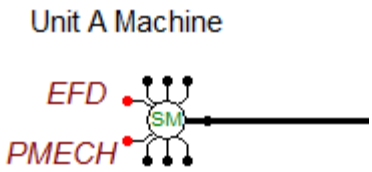

Figure B.7: Unit A Generator Implementation

Unit B Implementation

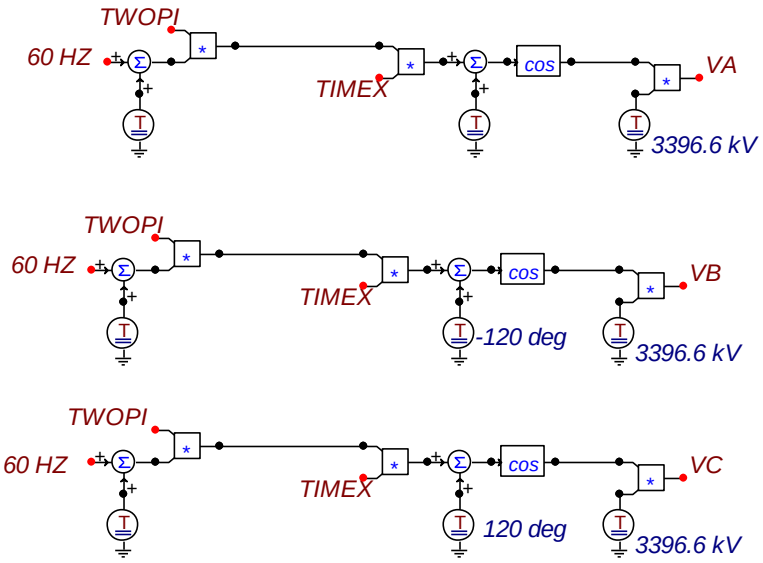

Figure B.8: Unit B Generator Implementation

Thevenin Source Implementation

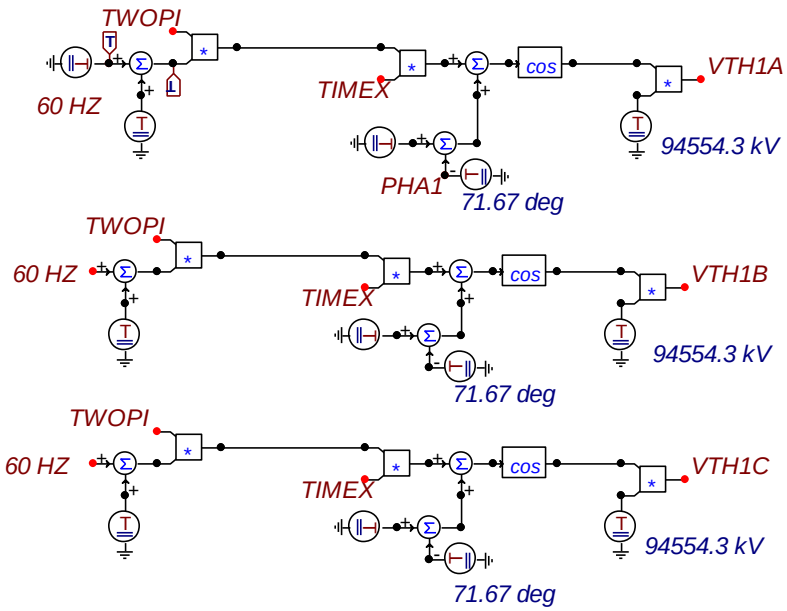

Figure B.9: Thevenin Source – at PCC1 Implementation

An Example of one of the Phase Locked Loop Control Circuits

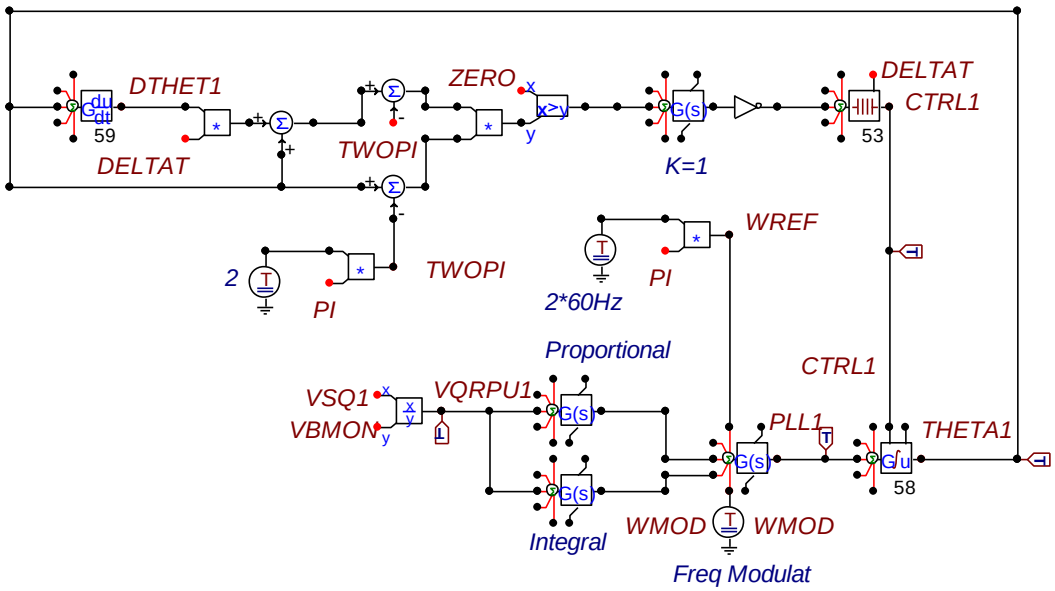

Figure B.10: PLL Control Circuit at PCC 1

An Example of a Frequency Measurement Circuit

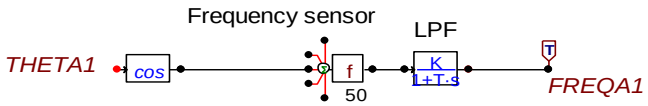

Figure B.11: Frequency Measurement at PCC 1

Islanding Detection (over/under voltage) Scheme

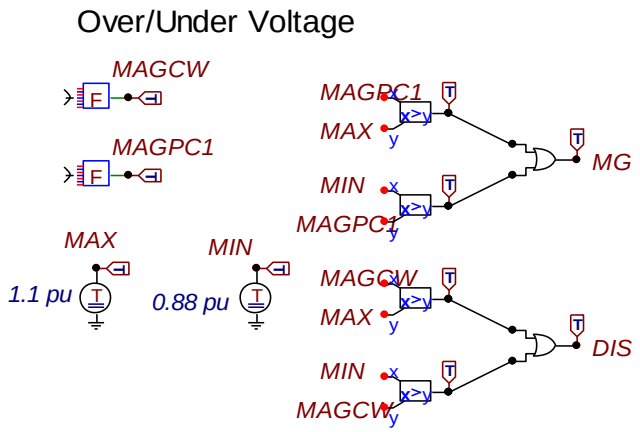

Figure B.12: OUV Scheme at PCC 1

Islanding Detection (over/under frequency) Scheme

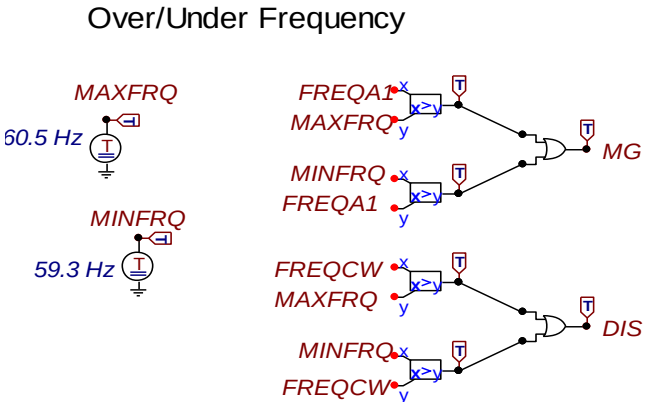

Figure B.13: OUF Scheme at PCC 1

Negative Sequence Filter:

During SLG fault condition, the second harmonic due to the negative sequence voltage was removed by the filter that is shown in Figure B.14.

The voltage measurements for the PLL were entered to the negative sequence filter with a transfer function as shown in equation (B.2)

$$H(s) = \frac{S^2 + 568489.214\ Hz^2}{S^2 + 350\ Hz + 568489.214\ Hz^2} \quad \text{(B.2)}$$

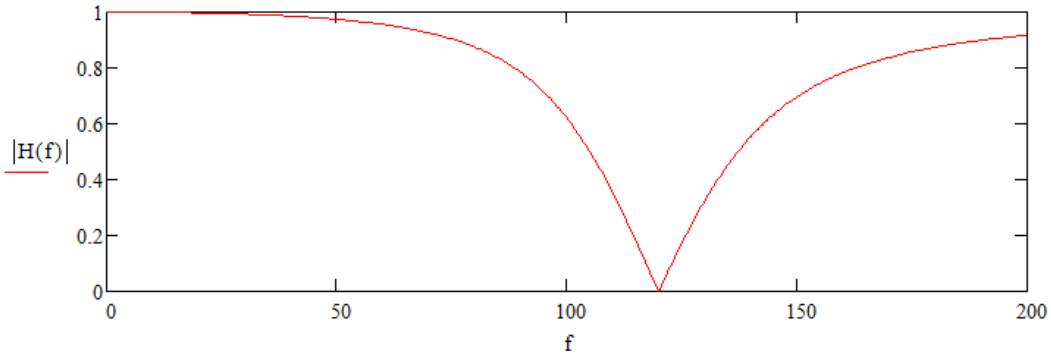

Figure B.14: Negative Sequence Filter